Deep–Sea Research II 220 (2025) 105459

Contents lists available at ScienceDirect

Deep-Sea Research Part II

journal homepage: www.elsevier.com/locate/dsr2

Contrasting trends of the ocean CO_2 sink and pH in the agulhas current system and the Mozambique basin, south-western Indian ocean (1963–2023)☆

Nicolas Metzl [a,*], Claire Lo Monaco [a], Guillaume Barut [a,b], Jean-François Ternon [c]

[a] Laboratoire LOCEAN/IPSL, Sorbonne Université-CNRS-IRD-MNHN, Paris, 75005, France
[b] Takuvik Joint International Laboratory, Université Laval/CNRS, 1045, Av. de La Médecine, Québec, G1V 0A6, Canada
[c] MARBEC, Université de Montpellier, CNRS, Ifremer, IRD, 34203, Sète, France

ARTICLE INFO

Handling Editor: Prof. J Aristegui

Keywords:
Air-sea CO2 fluxes
Ocean acidification
Indian ocean
Mozambique basin
Agulhas current

ABSTRACT

We describe new observations of the oceanic carbonate system in the South-Western Indian Ocean obtained in January 2021 (OISO-31 cruise) and May 2022 (RESILIENCE cruise). To evaluate the decadal trends and drivers of fugacity of CO_2 (fCO_2), air-sea CO_2 fluxes, dissolved inorganic carbon (C_T) and pH, we used available data in this region over 1963–2023 and compared the results in the Mozambique Basin and in the Agulhas region near the African coast. Over 1995–2023, we found a faster fCO_2 increase in the Mozambique basin (2.03 ± 0.07 µatm.yr^{-1}) compared to the coastal zone (1.37 ± 0.07 µatm.yr^{-1}). The temporal change of anthropogenic CO_2 concentrations estimated in subsurface enables to reconstruct the carbonate system properties since the 1960s. In the Mozambique Basin the CO_2 sink increased slightly over 1960–2022 with a maximum observed in May 2022 (-2.4 mmolC.m^{-2}.d^{-1}). In the coastal zone, the ocean CO_2 sink increased from near equilibrium in the 1960s to a maximum observed in May 2022 (-4.2 mmolC.m^{-2}.d^{-1}). In both regions, we found a decrease of pH, most pronounced in the open ocean zone (-0.020 ± 0.001.$decade^{-1}$ over 1995–2023). The lowest pH of 8.04 was observed in January 2021, 0.11 lower than in the 1960s. The increase of the CO_2 sink and the decrease of pH were mainly driven by anthropogenic CO_2 uptake, with about 10% due to the ocean warming.

1. Introduction

The ocean plays a major role in reducing the impact of climate change by absorbing more than 90% of the excess heat in the climate system (Cheng et al., 2020) and about 25% of human released CO_2 (Friedlingstein et al., 2022, 2023). The oceanic CO_2 uptake also changes the chemistry of seawater reducing its buffering capacity (Revelle and Suess, 1957) and leading to a process known as ocean acidification (OA) with potential impacts on marine organisms (Fabry et al., 2008; Doney et al., 2009, 2020). Although important international effort have been conducted to synthetize fCO_2 observations (Bakker et al., 2016) and their use to reconstruct fCO_2 fields and air-sea CO_2 fluxes (Rödenbeck et al., 2015), there are still large uncertainties on the ocean CO_2 sink estimate at global scale (De Vries et al., 2023; Friedlingstein et al., 2022, 2023) and in coastal zones (Resplandy et al., 2024). At seasonal scale large differences between observations and models were identified leading to difference of the global coastal ocean CO_2 sink up to 60% (Resplandy et al., 2024). To reduce these uncertainties, it is thus important to better document the carbonate system (CS) for comparing and correct Ocean Biogeochemical Global Models (OBGM) and climate/carbon models (CMIP) used to predict future changes of the ocean states including ocean acidification (e.g. Jiang et al., 2023) and their impact on the marine ecosystems (Doney et al., 2020; Kwiatkowski et al., 2020). Coastal waters experienced enhanced ocean acidification due to increase CO_2 uptake (Bourgeois et al., 2016; Laruelle et al., 2018; Roobaert et al., 2024). As opposed to open ocean zones, it is difficult to detect acidification trends in the heterogeneous coastal waters due to combined effects of anthropogenic CO_2, ocean warming, local

☆ Submitted 15/8/24 to: DSR II special issue, VSI: IIOE-2 Volume 7: 'The 2nd International Indian Ocean Expedition (IIOE-2): Motivating New Exploration in a Poorly Understood Basin (Volume 7)'. Revision, 17/12/24.

* Corresponding author.
E-mail addresses: nicolas.metzl@locean.ipsl.fr (N. Metzl), claire.lomonaco@locean.ipsl.fr (C. Lo Monaco), guillaume.barut@takuvik.ulaval.ca (G. Barut), jean-francois.ternon@ird.fr (J.-F. Ternon).

https://doi.org/10.1016/j.dsr2.2025.105459
Received 14 August 2024; Received in revised form 17 December 2024; Accepted 13 January 2025
Available online 17 January 2025

anthropogenic inputs through rivers and from air pollution (e.g. Sarma et al., 2015; Sridevi and Sarma, 2021), as well as due to variability of upwelling and biological processes like observed in the Western Boundary Current (WBC) such as the Agulhas Current system investigated here. In this region, identified as MARCATS #25 (Margins and CATchment Segmentation, Laruelle et al., 2013), only one study evaluated the CO_2 fluxes based on fCO_2 data (Arnone et al., 2017). As noted by these authors, 8 years of data (in 2005–2012) enabled to estimate the mean flux in this region, a CO_2 sink of -1.65 ± 0.04 molC.m^{-2}.yr^{-1}, but cannot separate the natural decadal and anthropogenic signal. Concerning the ocean acidification in African coastal zones observations were only available in the western side (González-Dávila et al., 2017): these authors estimated a pH decrease of -0.03 ± 0.01.decade^{-1} but this was evaluated for a short period (2005–2012). Based on fCO_2 data and using Alkalinity/Salinity (A_T/S) relationship, Lauvset et al. (2015) estimated a pH trend in the Indian Ocean Subtropical biome (STPS) of -0.024 ± 0.004.decade^{-1} for the period 1981–2011. Recently, reconstructed sea surface carbonate system properties for the period 1985–2021 suggested pH trend of between -0.020 and -0.017.decade^{-1} in the South-Western Indian Ocean (Chau et al., 2024). This analysis, along with other data-products and ocean models was then used to quantify the trends and drivers of the ocean acidification in the Indian Ocean (Chakraborty et al., 2024). These authors highlighted an acceleration of the pH trend from -0.011 (± 0.00).decade^{-1} in 1980–1989 to -0.019 (± 0.004).decade^{-1} in 2010–2019. To investigate the long-term changes of pH in the Indian Ocean Madkaiker et al. (2023) also used outputs from ocean models and found that over 1961–2010 the decrease of pH was mainly driven by the increase of dissolved inorganic carbon (69%) with a significant contribution of the warming (14%). In the Mozambique Channel, Lo Monaco et al. (2021) estimated a pH decrease of -0.023 ± 0.005.decade^{-1} over 1995–2019. These results highlight the contrasting pH trend between open ocean and coastal zones and depending the period. In a recent review of the biogeochemistry in the Indian Ocean, Ghosh et al. (2024) concluded that "research on ocean acidification in the Indian Ocean is in its early stages" and that "coordinated multidisciplinary chemical and biological observational approaches are needed to document the status of ocean acidification in the high seas and coastal environments". In this context we present new observations obtained in 2021 and 2022 as part of the OISO-31 and RESILIENCE cruises conducted in the South Western Indian Ocean, the Mozambique Basin, the Agulhas current system and African coastal zone. To investigate the long-term change of the air-sea CO_2 fluxes and of the carbonate system we also used historical data in this region obtained over 1963–2023.

2. Data selection and methods

2.1. Data selection

The OISO-31 (January–March 2021) and RESILIENCE (May 2022) cruises were conducted in the South-Western Indian Ocean. Part of these cruises followed the same track in the Madagascar and the Mozambique Basins (Fig. 1). To explore the long-term change of the carbonate system in this region, we used the SOCAT data, version v2024 (Bakker et al., 2016, 2024, Fig. 1c, Supp. Mat. Table S1a) and the GLODAP data, version v2023 (Lauvset et al., 2024, Supp. Mat. Table S1b). As we used salinity in the carbonate system calculations and salinity was not quality controlled in SOCAT, we have checked the salinity and found bias for few cruises (in 2011 and 2012); for these cruises we thus used the World Ocean Atlas (WOA) salinity as listed in the SOCAT data files (Antonov et al., 2006; Pfeil et al., 2013).

2.2. Methods

The methods for surface underway fCO_2 and biogeochemical properties (Oxygen, A_T, C_T, nutrients) were described in previous studies (e.g. Lo Monaco et al., 2021; Metzl et al., 2022). Here we briefly recall the methods for underway fCO_2 and water-column observations.

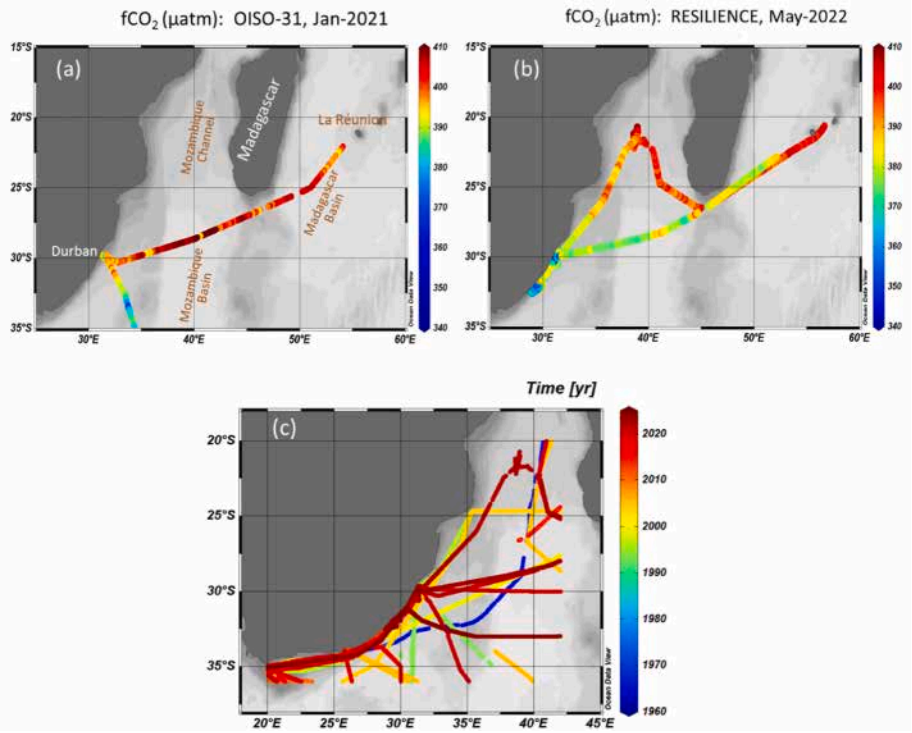

Fig. 1. Maps of OISO-31 cruise (a) and RESILIENCE cruise (b) conducted in January 2021 and April–May 2022; color code is for sea surface fCO_2 (µatm). (c) Tracks of cruises in the SOCAT data-base, v2024 (Bakker et al., 2016, 2024); color code is for Year (1963–2023). Figures produced with ODV (Schlitzer, 2018).

2.2.1. Surface fCO_2 and A_T C_T data

For fCO_2 measurements during OISO-31 (2021) and RESILIENCE (2022) cruises, sea-surface water was continuously equilibrated with a "thin film" type equilibrator thermostated with surface seawater (Poisson et al., 1993) and xCO2 in the dried gas was measured with a non-dispersive infrared analyzer (NDIR, Siemens Ultramat 6F). Standard gases for calibration (279.31 ppm or 267.39 ppm, 350.75 ppm or 374.92 ppm and 489.09 ppm) were measured every 6 h. The fCO_2 in situ data were corrected for warming using corrections proposed by Copin-Montégut (1988, 1989). Note that when incorporated in the SOCAT data-base, the original fCO_2 data are recomputed (Pfeil et al., 2013) using temperature correction from Takahashi et al. (1993). Given the very small difference between equilibrium temperature and sea surface temperature (+0.088 ± 0.066, n = 6416, on average for the RESILIENCE cruise in 2022), the fCO_2 data from SOCAT used in this analysis (Bakker et al., 2024) are almost identical (within 1 µatm) to the original fCO_2 values (Lo Monaco and Metzl, 2024).

Total alkalinity (A_T) and dissolved inorganic carbon (C_T) were measured continuously in surface water (3–4 sample/hour) using a potentiometric titration method (Edmond, 1970) in a closed cell. For calibration, we used the Certified Referenced Materials (CRMs, Batch #182 and 191 for OISO-31) provided by Pr. A. Dickson (SIO, University of California). The repeatability of A_T and C_T measurements was evaluated from duplicate analyses of continuous sea surface sampling at the same location (when the ship was stopped). The mean differences of 343 duplicates were better than 3 µmol kg^{-1} for A_T and C_T (Supp. Mat. Table S2). We estimated the accuracy for both A_T and C_T better than 3 µmol kg^{-1}. The A_T and C_T data from OISO-31 cruise are available at NCEI/OCADS (Lo Monaco et al., 2023). These data offered comparisons and validation for the calculations of the carbonates properties using fCO_2 data and A_T/Salinity relationship.

2.2.2. Carbonate system calculation and A_T/salinity relationship

When two of the carbonate system properties are measured (fCO_2, A_T, C_T and pH) they can be used to calculate other species including the saturation state of aragonite and calcite (Ω_{Ar}, Ω_{Ca}). Here we have measurements of either fCO_2 underway data or A_T and C_T from both underway sampling and in the water column at stations. To calculate pH and C_T from the fCO_2 data we used the CO2sys program (version CO2sys_v2.5, Orr et al., 2018) developed by Lewis and Wallace (1998) and adapted by Pierrot et al. (2006) with K1 and K2 dissociation constants from Lueker et al. (2000) and KSO4 constant from Dickson (1990). The total boron concentration is calculated according to Uppström (1974). When using fCO_2 data to derive pH or C_T, one needs A_T concentrations that can be derived from salinity (e.g. Millero et al., 1998; Lauvset et al., 2015; Lo Monaco et al., 2021). Here we used the underway surface A_T observations obtained in 2004 (OISO-11) and 2021 (OISO-31) and compared the A_T/Salinity relationship with that derived from stations data in the surface layer (0–20m) in 1987–2021 in this region (Fig. 2). We thus obtained two relationships:

From underway data:

A_T (µmol.kg^{-1}) = 53.2626 (±2.23) * *Salinity* + 432.359 (±78.79) (n = 408, r2 = 0.58) (Eq. (1))

From Stations data:

A_T (µmol.kg^{-1}) = 66.1773 (±2.55) * *Salinity* −23.8222 (±90.55) (n = 205, r2 = 0.77) (Eq. (2))

Both relationships lead to the same results for the C_T or pH calculations and we used the relationship from the stations (Eq. (2)) assuming there is no long-term change in salinity and alkalinity in this region. The validation of the calculation with underway surface measurements in 2021 is shown in Fig. S1 (Table S3). Given the errors in the CO_2sys calculations (errors on constants K1, K2 and measurements, Orr et al., 2018) we consider the A_T/Salinity relationship valid to calculate accurately the C_T concentrations and pH in this region. Along the OISO-31 track, the difference between calculated and measured C_T is only 3.2 µmol kg^{-1} (compared to the theoretical error of 7 µmol kg^{-1} when using fCO_2 and A_T data). This supports the use of the selected A_T/S relationship for carbonate system calculations based on all fCO_2 data available over 1963–2023 in the investigated region.

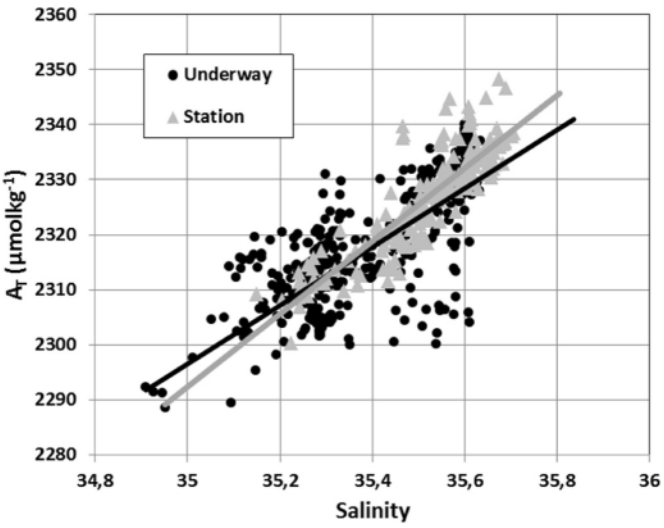

Fig. 2. Relationship of A_T (µmol kg^{-1}) versus Salinity deduced from surface A_T data obtained during OISO 11 and OISO-31 cruises in 2004 and 2021 (black circles) or from station data (at depth 0–20m from GLODAP data, grey triangles) in the in the South-Western Indian Ocean (zone 20–45°E/20–40°S). The relationship (grey line, A_T = 66.1773 * Salinity - 23.8222) is used to calculate pH and C_T concentrations in this region. A_T underway data are available at NCEI/OCADS (https://www.ncei.noaa.gov/access/ocean-carbon-data-system/oceans/VOS_Program/OISO.html).

3. Results

3.1. Distribution during OISO-31 (January 2021) and RESILIENCE (May 2022)

The RESILIENCE cruise started from La Réunion in late April and went back to La Réunion in late May (Fig. 1). This cruise had two Legs: Leg 1 in the central Mozambique Channel (not included in this paper), and Leg 2 along the east coast of South Africa. The OISO-31 cruise also started from La Réunion in January 2021 and reached the African coast before moving at higher latitudes in the Southern Indian Ocean. Here we compare the data obtained along the same track between La Réunion and the African coast (Fig. 3). In January 2021, during the warm season, fCO_2 was near equilibrium. In May 2022, the ocean was colder and acted as a CO_2 sink for the atmosphere during this season ($\Delta fCO2 < 0$, where $\Delta fCO2 = fCO_2^{ocean} - fCO_2^{atm}$). This is coherent with previous studies and ΔfCO2 climatology (Poisson et al., 1993; Takahashi et al., 2009; Fay et al., 2024). In the subtropical Indian ocean north of 26°S, C_T and A_T concentrations were lower in May 2022 because the salinity was also lower and thus no difference was observed in salinity normalized C_T and A_T. Consequently the low fCO_2 in May was mainly driven by temperature as generally observed in subtropics (e.g. Metzl et al., 1998; Sabine et al., 2000).

For both seasons the C_T concentrations were lower around 26°S south of Madagascar (1970 µmol kg^{-1}) when crossing a high productivity region (Fig. S2). The presence of low C_T concentrations was also observed around 40–43°E/28°S in 2021 and 2022 and were confirmed with direct C_T measurements in 2021 (Fig. S1). This was linked to the presence of a cyclonic eddy (as recorded in SST, Fig. 3) and a bloom occurring south-west of Madagascar (Fig. S2) associated to productive areas probably linked to N_2-fixers such as diazotrophs Trichodesmium (Poulton et al., 2009; Chowdhury et al., 2024). These local events changed slightly ΔfCO_2 (stronger sink) and C_T, but have no large impact when properties were averaged over the domain (Table 1). The highest

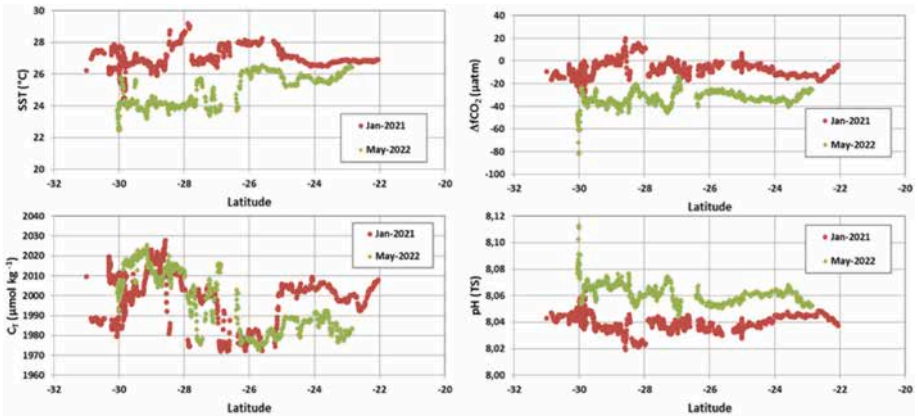

Fig. 3. Distribution of sea surface temperature, ΔfCO_2, C_T, and pH in January 2021 (red) and in May 2022 (green) along the same track in the southwestern Indian Ocean (from La Réunion to Durban). Average values are listed in Table 1.

Table 1
Average of properties observed or calculated from fCO_2 underway data in January 2021 (OISO-31) and in May 2022 (RESILIENCE) along the same track in the southwestern Indian Ocean (See Fig. 3). The mean values were estimated for the band 22–26°S, 26–31°S and 22–31°S. SD are in bracket. Nb is the number of data for each region. The difference (January minus May) are indicated.

Date	Region	SST °C	SSS psu	fCO_2 µatm	ΔfCO_2 µatm	A_T µmol.kg^{-1}	C_T µmol.kg^{-1}	pH TS	Ω_{Ca}	Ω_{Ar}	Nb
Jan 2021	22-26°S	27.112	35.401	402.8	−7.4	2318.9	1998.9	8.039	5.47	3.63	436
		(0.429)	(0.122)	(4.8)	(4.8)	(8.1)	(8.4)	(0.005)	(0.03)	(0.02)	
Jan 2021	26-31°S	26.807	35.412	403.4	−6.8	2319.6	2002.3	8.039	5.43	3.60	1154
		(0.739)	(0.172)	(7.9)	(7.9)	(11.4)	(14.2)	(0.006)	(0.10)	(0.07)	
Jan 2021	22-31°S	26.890	35.409	403.2	−7.0	2319.5	2001.4	8.039	5.44	3.61	1590
		(0.682)	(0.160)	(7.2)	(7.2)	(10.6)	(12.9)	(0.006)	(0.09)	(0.07)	
May 2022	22-26°S	25.904	35.099	381.0	−31.6	2298.9	1982.9	8.058	5.39	3.56	279
		(0.379)	(0.091)	(3.8)	(3.8)	(6.0)	(5.2)	(0.004)	(0.03)	(0.02)	
May 2022	26-31°S	24.223	35.365	377.7	−34.9	2316.5	2008.1	8.065	5.24	3.45	599
		(0.647)	(0.192)	(7.2)	(7.2)	(12.7)	(11.9)	(0.008)	(0.09)	(0.07)	
May 2022	22-31°S	24.758	35.280	378.7	−33.8	2310.9	2000.1	8.062	5.29	3.49	878
		(0.972)	(0.208)	(6.5)	(6.5)	(13.7)	(15.6)	(0.007)	(0.11)	(0.08)	
Diff.	22-26°S	1.208	0.303	21.8	24.2	20.0	16.0	−0.018	0.08	0.07	
Diff.	26-31°S	2.583	0.047	25.7	28.1	3.1	−5.8	−0.025	0.18	0.15	
Diff.	22-31°S	2.133	0.129	24.5	26.9	8.5	1.3	−0.023	0.15	0.12	

calculated C_T concentrations (2020 µmol kg^{-1}) were observed around 29°S in 2021 and 2022 (Fig. 3). This is a location where the ocean with high temperature and high C_T was a CO_2 source in January (ΔfCO_2 close to +20 µatm). This is a local variation and we note that ΔfCO_2 was very homogeneous along this track in 2021 and 2022 (Fig. 3, Table 1), except near the coast where we observed a much stronger sink, ΔfCO_2 up to −80 µatm in May 2022.

During the RESILIENCE cruise (Leg 2), the coastal zone was investigated in detail at 2 locations: in an "Active Durban Eddy" (ADE, 4–7 May) located around 30°S and in an "Old Durban Eddy" (ODE 8–15 May) located at 32°S near the Protea Banks. The Durban Eddy at ADE was no longer active when the ship arrived on site while it has been clearly identified from satellite imagery a few days before. ADE are known to be regularly occurring temporary structures (~10 days) that

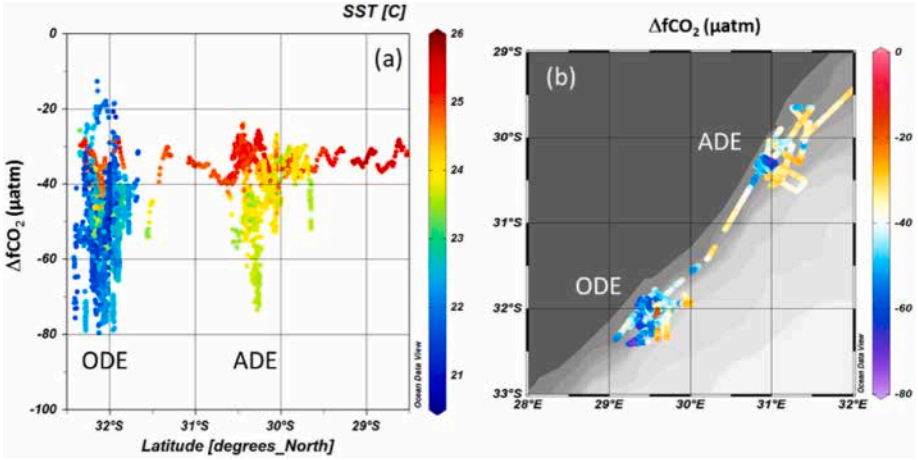

Fig. 4. Distribution of ΔfCO_2 (µatm) during the RESILENCE cruise in May 2022 along the African coast. In (a) color code is for SST (°C). In (b) color code is for ΔfCO_2 (µatm). "ADE" and "ODE" identifies the locations of the Active Durban Eddy and the Old Durban Eddy investigated during the cruise. In May 2022, the ocean was always a CO_2 sink in this region ($\Delta fCO_2 < 0$). Figures produced with ODV (Schlitzer, 2018).

are then transported southwestwards through the Agulhas Current influence, to become ODE until they lose their kinetic energy and disappear (Guastella and Roberts, 2016). The distribution of ΔfCO_2 in May 2022 in this region is presented in Fig. 4. The ocean was always a CO_2 sink ($\Delta fCO_2 < -20$ µatm) as previously observed (Arnone et al., 2017). The lowest ΔfCO_2 (−60 to −80 µatm) were observed in the ADE and ODE rings. There was no clear link with the temperature or salinity and the low ΔfCO_2 observed at 30 and 32°S were driven by primary production. This is supported by the variation of surface Chl-a concentrations that present maxima occurring at 29°S and 31-30°S in April 2022 (before the cruise) and in May 2022 at 32°S (Fig. S3). The observed ΔfCO_2 minima (<-50 µatm at 29.5°S, 30.5°S and 32°S, Fig. 4) occurred where the sea surface Chl-a was high (up to 3 mg m^{-3}). This supports that biological activity was the main driver of the fCO_2 variations in May 2022 along the coast. This also suggests that biological ADE signature was still present at the time of the sampling while the eddy itself was no longer identifiable on site.

The contrasting fCO_2 or ΔfCO_2 distribution near the coast and offshore described above was observed for most of cruises since 1963 (Fig. 5). The low ΔfCO_2 in April–May as observed in 2022 (up to −80 µatm) was recorded only once (in late April 2018 at 30°S/31°E, $\Delta fCO_2 = -50$ µatm). For most of the seasons, the high fCO_2 variability occurred west of 32°E, i.e. west of the Agulhas current. The data also indicate a clear increase of fCO_2 since 1963 in this domain (Fig. 5). What is the decadal variability of fCO_2 and pH in this region and is this signal driven by anthropogenic CO_2 uptake or also due to natural variability? To explore the long-term trends of the carbonate system and given the spatial and seasonal variability of fCO_2 in this region, we separated the domain in two regions, one in the Mozambique Basin east of 32°E (open ocean) and one near the coast (in the ADE and ODE regions).

3.2. Trends in the Mozambique basin

To evaluate the trend in the Mozambique Basin, we have selected the data in the region east of 32°E where fCO_2 was homogeneous each year and season (Fig. 5). The mean values in this region since 1963 are presented in Fig. 6 and Table 2. The fCO_2 seasonality being large of around 40 µatm between summer and winter it is appropriate to select the same season for the trend analysis. We thus used the data available in April–May (only in 2018, 2019 and 2022), i.e. the same season as for the cruise conducted in 1963 (Keeling and Waterman, 1968). Over 1963–2022 the oceanic fCO_2 trend of $+1.79 \pm 0.13$ µatm.yr^{-1} is close to the atmospheric trend ($+1.66 \pm 0.03$ µatm.yr^{-1}). This explained that the CO_2 sink was almost the same in May 1963 and May 2022 ($\Delta fCO2 = -33.1$ and −32.3 µatm respectively). This is also close to the climatology in May in this region ($\Delta fCO2 = -20.4 \pm 9.9$, Fay et al., 2024).

As observed in the global ocean (Cheng et al., 2024) the South-West Indian Ocean experienced a long-term warming here evaluated at $+0.120 \pm 0.009$ °C.$decade^{-1}$ since the 1960s (Fig. S4). As fCO_2 is sensitive to temperature we corrected the fCO_2 data to normalized temperature at 25 °C following Takahashi et al. (1993):

$$fCO_2^{25} = fCO_2^{SST} * \text{EXP}\ (0.0423*(25\text{-}SST)) \quad (3)$$

The warming would have increase fCO_2 by +9 µatm in 59 years, a signal included in the observations. When normalizing fCO_2 at 25 °C, the trend of fCO_2^{25} is $+0.90 \pm 0.25$ µatm.yr^{-1}, i.e. less than derived from fCO_2. To explain what drive the fCO_2 (and pH) change, one must evaluate the anthropogenic CO_2.

To estimate the evolution of the anthropogenic CO_2 concentrations (C_{ant}) we selected the stations available from 1987 to 2021. The C_{ant} concentrations were calculated using the TrOCA method (Touratier et al., 2007) in the layer 100–150m as the back-calculation methods are not suitable for evaluating C_{ant} concentrations in surface waters due to gas exchange and biological activity. To estimate the C_{ant} trend, the concentrations were averaged for each period (Fig. 7a). As expected, the C_{ant} concentrations increase progressively from 28.3 ± 3.7 µmol kg^{-1} in 1987 to 62.2 ± 4.2 µmol kg^{-1} in 2021. The increase from 1995 to 2003 of +6.9 µmol kg^{-1} is in the range of the averaged C_{ant} increase of $+7.7 \pm 0.5$ µmol kg^{-1} observed between 1995 and 2003/2004 in the Indian Central Water (ICW) (Murata et al., 2010). Our results over 1987–2021 lead to a trend of C_{ant} of $+1.03 \pm 0.14$ µmol kg^{-1} yr^{-1} (Table 3) and, as expected, the C_{ant} concentrations in the ocean are positively related to atmospheric CO_2 (slope $+0.512 \pm 0.050$ µmol kg^{-1} µatm^{-1}, Fig. 7b). Interestingly the slope observed in the South-Western Indian Ocean over 1987–2021 is very close to that observed in the South Atlantic Central Water in the South Atlantic over 1972–2019 ($+0.51 \pm 0.02$ µmol kg^{-1} µatm^{-1}, Fontela et al., 2021). Furthermore, the trend of C_{ant} in the Mozambique Basin is also comparable to that derived further east at 30°S-55°E in the Madagascar Basin between 1978 and 2020 ($+1.05 \pm 0.08$ µmol $kg^{-1}.yr^{-1}$, Metzl et al., 2022) indicating this signal is homogeneous in the southern Atlantic and Indian oceans at these latitudes.

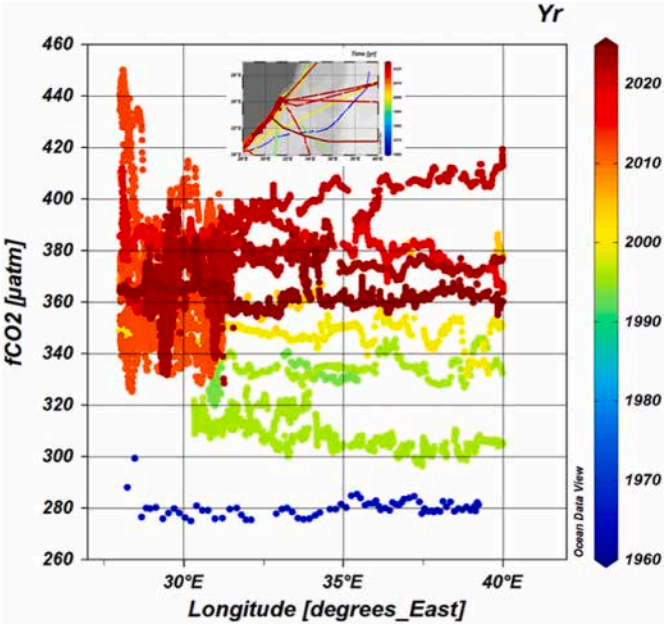

Fig. 5. Distribution of sea surface fCO_2 (µatm) in the eastern African coastal zone and offshore for all cruises over 1963–2023 in the SOCAT data-base, v2024 (Bakker et al., 2016, 2024); color code is for Year. This includes the OISO-31 and RESILIENCE cruises. The selected tracks are indicated in the insert map. Figures produced with ODV (Schlitzer, 2018).

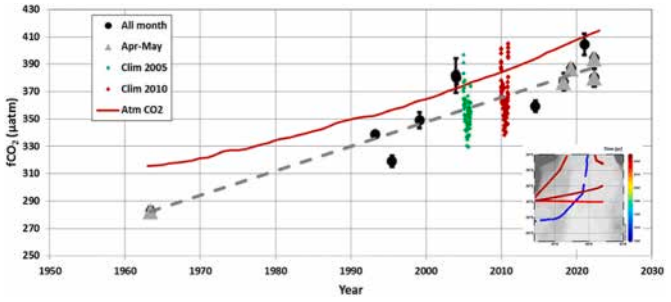

Fig. 6. Time-series of monthly mean fCO_2 (µatm, black dots for all season and grey triangles for April–May) in the Mozambique Basin (region 24°S-35°S/32°E–42°E). The red curve is the atmospheric fCO_2. The monthly climatology for a reference year 2005 or 2010 (Takahashi et al., 2014; Fay et al., 2024) is also plotted (green and red diamonds) highlighting the seasonality in this region. For the period April–May the oceanic fCO_2 increase of $+1.79 \pm 0.13$ µatm.yr^{-1} (dashed grey line) is close to the atmospheric increase. The selected tracks in April–May are indicated in the insert map produced with ODV (Schlitzer, 2018). The mean monthly values and standard deviations are listed in Table 2.

Table 2
Average of properties measured or calculated from the sea surface underway fCO_2 data in the Mozambique Basin. The mean values were estimated for the box 24tbox24°S-35°S/32°E−42°E (insert map in Fig. 6). SD are in bracket. Nb is the number of data for each region. Bold value identifies anomalies in 2019.

Year	Month	NB	SST	SSS	fCO_2	A_T	C_T	pH	Ω_{Ca}	Ω_{Ar}
1963	5	54	22.133	35.369	282.3	2316.8	1963.8	8.168	5.90	3.86
			(1.027)	(0.156)	(3.5)	(10.3)	(13.1)	(0.006)	(0.11)	(0.08
1993	3	10	25.486	35.437	338.6	2321.3	1977.0	8.102	5.82	3.84
			(0.034)	(0.016)	(1.9)	(1.0)	(1.7)	(0.002)	(0.01)	(0.01)
1995	6	2876	23.290	35.489	319.1	2324.7	1985.9	8.125	5.70	3.74
			(0.702)	(0.053)	(4.2)	(3.5)	(7.0)	(0.005)	(0.09)	(0.06)
1999	2	403	26.333	35.388	348.9	2318.1	1973.8	8.090	5.84	3.86
		(0.06)	(0.106)	(5.7)	(7.0)	(10.4)	(0.005)	(0.08)	(0.06)	(0.524)
2003	12	450	27.137	35.297	381.9	2312.1	1982.1	8.057	5.63	3.74
			(1.006)	(0.067)	(12.5)	(4.4)	(6.5)	(0.012)	(0.07)	(0.06)
2004	1	195	27.159	35.344	380.1	2315.1	1983.2	8.059	5.66	3.76
			(0.413)	(0.057)	(4.8)	(3.8)	(5.5)	(0.005)	(0.05)	(0.04)
2014	7	882	23.506	35.342	359.3	2315.0	2002.6	8.083	5.29	3.48
		(0.06)	(0.054)	(4.0)	(3.6)	(7.0)	(0.004)	(0.08)	(0.06)	(0.683)
2018	4	945	25.126	35.500	377.1	2325.5	2006.5	8.065	5.42	3.58
			(1.320)	(0.178)	(6.4)	(11.8)	(15.2)	(0.007)	(0.14)	(0.11)
2019	4	120	**27.290**	**35.328**	386.8	**2314.1**	**1985.1**	8.053	5.62	3.73
			(0.159)	**(0.095)**	(3.5)	**(6.3)**	**(4.6)**	(0.004)	(0.03)	(0.02)
2021	1	757	26.676	35.509	404.6	2326.1	2008.7	8.039	5.42	3.60
			(0.588)	(0.118)	(7.9)	(7.8)	(11.1)	(0.006)	(0.08)	(0.06)
2022	4	173	26.407	35.412	394.2	2319.6	2000.8	8.048	5.44	3.60
			(0.400)	(0.039)	(3.2)	(2.6)	(3.2)	(0.003)	(0.08)	(0.06)
2022	5	720	24.912	35.459	380.3	2322.8	2008.2	8.062	5.35	3.53
			(1.039)	(0.084)	(6.6)	(5.6)	(7.8)	(0.007)	(0.13)	(0.09)

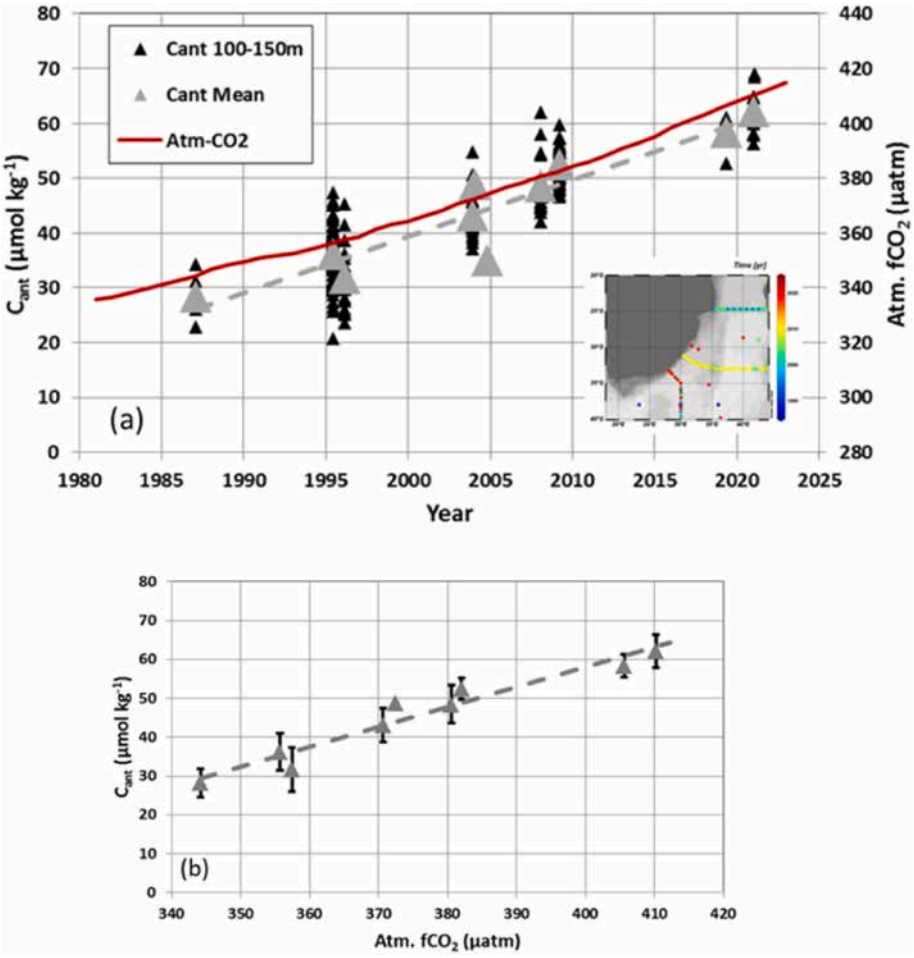

Fig. 7. (a) Time-series of anthropogenic CO_2 concentrations (C_{ant}) over 1987–2021 estimated in subsurface (layer 100–150m) from the GLODAP-v2023 data (Lauvset et al., 2024) completed with OISO cruise in 2021 (location of selected stations in the insert map, color code is for year). The figure shows the C_{ant} concentrations calculated for each sample (black) and the C_{ant} averaged in the layer 100–150m for each period (grey triangles). Over the period 1987–2021, the C_{ant} trend is $+1.03 \pm 0.14$ µmol kg^{-1} yr^{-1} (dashed grey line). The red curve is the atmospheric fCO_2. (b): same data for C_{ant} versus atmospheric fCO_2 (slope = $+0.512 \pm 0.050$ µmol kg^{-1} µatm^{-1}).

Table 3
Trends of C_{ant} (µmol.kg^{-1}.yr^{-1}) in the Mozambique basin and the coastal zone in the layer 100–150 m for different periods. Standard-deviations are given in brackets.

Zone	Period	Trend Cant µmol.kg-1.yr-1
Mozambique Basin	1987–2021	+1.03 (0.14)
Mozambique Basin	1995–2021	+1.02 (0.11)
Coastal zone	1995–2021	+0.74 (0.21)

At constant temperature and alkalinity, the C_{ant} trend would lead to an increasing rate for fCO_2 of +1.58 µatm.yr^{-1} slightly lower than observed in surface waters (Fig. 6). For pH this would translate in the decrease of −0.017.decade^{-1}.

To interpret the observed fCO_2 change since the 1960s (Fig. 6) we assumed that the C_{ant} trend evaluated in subsurface represents the C_{ant} change in surface and we calculated the monthly C_T concentration over 1960–2022 by correcting C_T for each year using the relationship observed between C_{ant} and atmospheric CO_2 (Fig. 7b).

$$CT(t) + CT(t\text{-}1) + Cant(t)\text{-}Cant(t\text{-}1) \quad (4)$$

In this scenario we assumed that the C_T seasonality is not changing over

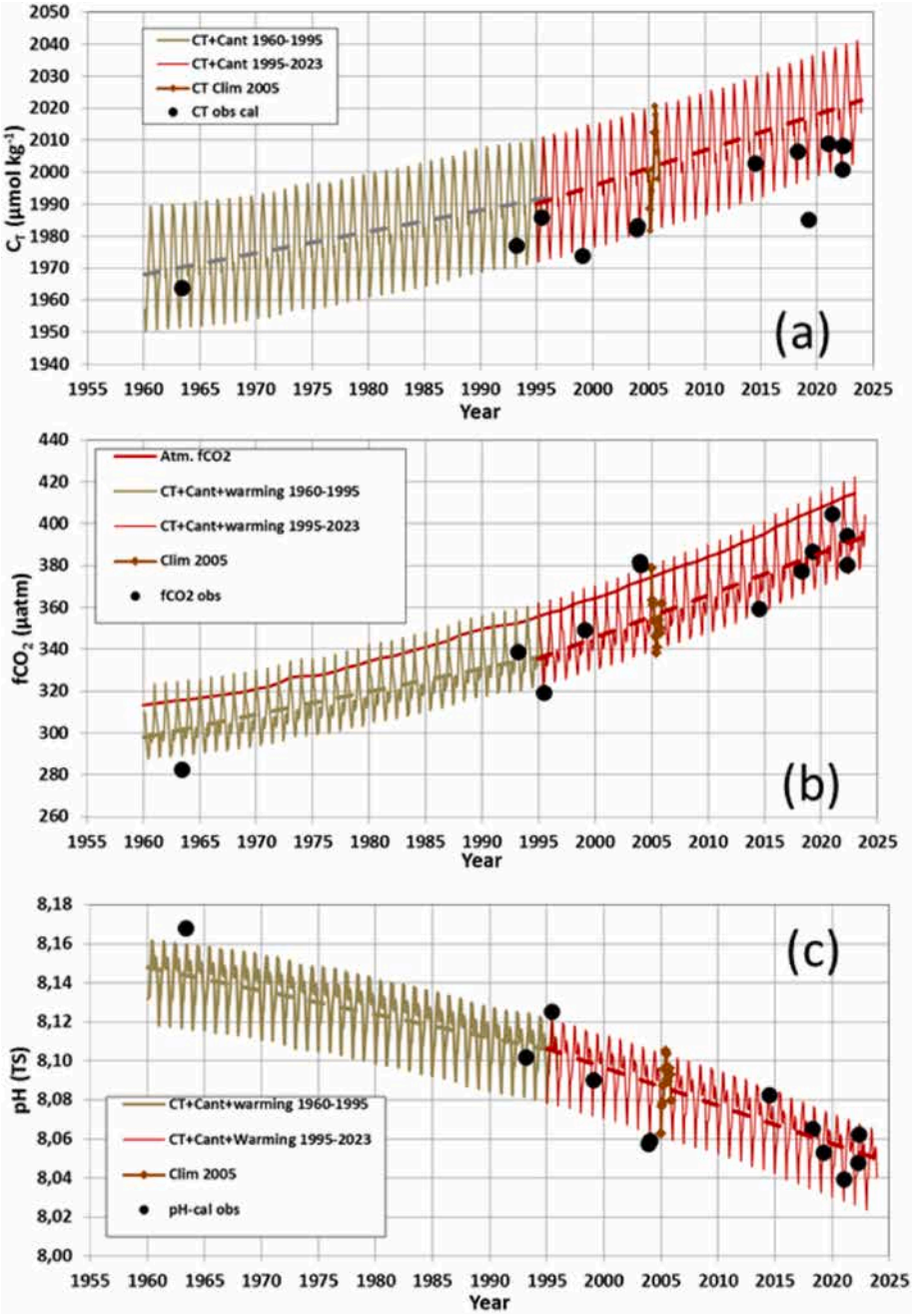

Fig. 8. Observed (black dots) and calculated time-series in the Mozambique Basin for (a) C_T (µmol.kg^{-1}), (b) fCO_2 (µatm) and (c) pH (TS). The lines show the evolution of the properties since 1960 corrected for C_{ant} where fCO_2, pH were recalculated using reconstructed C_T. Also shown the climatology for year 2005 (red diamonds, Takahashi et al., 2014). In (b) the red line is the atmospheric fCO_2. The trends (dashed line) are shown over 1960–1995 (brown) and 1995–2023 (red) (trends values are listed in Table 4).

time (Fig. 8a). The fCO_2 and pH are calculated using the reconstructed monthly C_T concentrations and the seasonal A_T based on the climatology (Takahashi et al., 2014). We also take into account the warming of +0.12 °C.decade^{-1} for fCO_2 and pH calculations (Fig. 8b and c). The reconstructed time series of C_T confirms that the C_{ant} accumulation explained most of the temporal C_T change observed in surface waters between 1963 and 2022.

The simulated C_T is in the range of observations except in April 2019 where the low C_T calculated from fCO_2 data was associated to salinity and temperature anomalies (Table 2). For other periods the mean difference of C_T between the reconstructed time-series and the observations is +6.6 ± 8.3 (n = 10) µmol kg^{-1}. Consequently, the results indicate that the increase of oceanic fCO_2 and the decrease of pH are driven by the anthropogenic CO_2 uptake and the ocean warming, the latter representing about 10% of the change in the recent decades (Table 4). The lowest pH of 8.04 was observed in January 2021. In May 2022 the pH was 8.062, i.e. -0.106 lower than in May 1963 (Fig. 8c) a difference equal to the mean change of −0.11 in the global ocean since the pre-industrial era (Jiang et al., 2019). The reconstructed time-series also shown that the trends are different depending the decade. The trends of C_T, fCO_2 and pH over the last three decades (1995–2023) were faster than over 1960–1995 (Table 4). These results are coherent with those investigated in the southern Mozambique Channel (Lo Monaco et al., 2021). In the Mozambique Basin where fCO_2 is rather homogeneous from time to time (Fig. 5), upwelling or biological activity have small impact on the C_T or the A_T variability, excepted when large bloom occurred south of Madagascar (Metzl et al., 2022) as also observed in 2021 and 2022 around 28°S (Fig. 3).

We now attempt to explore the fCO_2 and pH trends in the coastal zone where the interpretation is more obscure as the anthropogenic CO_2 and the warming effect on fCO_2 trends are probably masked by the variability in circulation near the Agulhas Current, the coastal upwelling or the biological activity as depicted from Chl-a (Fig. S3).

3.3. Trends in the coastal zone

As described above, the variability of fCO_2 in the Agulhas frontal system and near the coast was very large in May 2022 (Fig. 4). To explore the trends in this region we selected two regions, the ADE around 30°S and the ODE around 32°S that were visited during the RESILIENCE cruise. In the region 30–32°S/30–32°E there are few historical stations, available only in June 1995, March 2009 and January 2021. Over this period we estimated a C_{ant} trend of +0.74 ± 0.21 µmol kg^{-1} yr^{-1} in the layer 100–150m (Fig. S5) smaller than evaluated in the Mozambique Basin (+1.020 ± 0.106 µmol kg^{-1} yr^{-1} when using the same period, 1995–2021, Table 3). The relationship with atmospheric CO_2 is also different from the one deduced in the Mozambique Basin (C_{ant} = +0.342 ± 0.119 µmol kg^{-1} µatm^{-1}). Why the C_{ant} trend was lower in the coastal zone is not clear and for the reconstruction of the carbonate properties, we tested both relations. Although the C_{ant} trends in the Mozambique Basin and in the coastal zone are different, the C_T reconstructions seems almost the same (Fig. S6) but the comparison with observations suggested the reconstruction using C_{ant} trend in the coastal zone was better for this region (Fig. 9). The reconstructed C_T in the coastal region is in the range of the observations except in 2008 (at 32°S) and in 2021 (at 30°S) where the low C_T were linked to a warm anomaly. In May 2022 the concentration of reconstructed C_T (2014 µmol kg^{-1}) was almost the same as deduced from the fCO_2 data (2000 µmol kg^{-1} at 30°S in the ADE and 2012 µmol kg^{-1} at 32°S in the ODE). The recalculated fCO_2 was also very close to the observations in 2022 and 2023 (Fig. 9b). In June 1995 at 30°S we noticed lower observed fCO_2 (−10 µatm compared to the reconstruction) that might be linked to biological event but this cannot be confirmed with Chl-a data in 1995.

The trend of C_T in the coastal region was faster in the recent decade (1995–2023) but lower compared to the trend evaluated in the Mozambique Basin (Tables 4 and 5). Consequently, the annual rate of oceanic fCO_2 was lower in the coastal region (1.37 ± 0.07 µatm yr^{-1}) (Table 5) resulting in an increasing ocean CO_2 sink over 1995–2023 (ΔfCO_2 trend = −0.75 ± 0.07 µatm yr^{-1}). This contrasts with the results in the Mozambique Basin where the CO_2 sink was stable over 1995–2023 (ΔfCO_2 trend = −0.09 ± 0.07 µatm yr^{-1}, Fig. S7). In the coastal zone, we found that the ocean was near equilibrium ($-5 < \Delta fCO_2 < 0$ µatm) in the 1960s and moved to a sink of CO_2 during the last 2 decades (ΔfCO_2 <-20 µatm). The lowest ΔfCO_2 (−80 µatm) was observed in May 2022 in both the ADE and ODE regions (Fig. 4). The lowest pH (8.045) in the coastal zone was observed at 30°S in January 2021 (Fig. 9c). In May 2022 the pH of 8.071 was higher by 0.026, confirming the seasonal difference (May–January) of 0.03 in the climatology (Takahashi et al., 2014). Since 1995, the pH trend in the coastal region appeared slower (−0.014 ± 0.001.decade^{-1}) than in the Mozambique Basin (−0.020 ± 0.001.decade^{-1}). Our results in the eastern African coast is about half the pH trend of −0.03 ± 0.01.decade^{-1} estimated in the western coastal side but over a short period 2005–2012 (González-Dávila et al., 2017).

Table 4
Trends of sea surface C_T (µmol.kg^{-1}.yr^{-1}), fCO_2 (µatm.yr^{-1}) and pH (TS.decade^{-1}) based on observations (Obs.) and reconstruction (Rec.) for different periods in the Mozambique Basin (Fig. 8). Standard-deviations are given in brackets. Results for the reconstruction without warming are also listed (no warming).

Zone	Season	Trend CT µmol.kg-1.yr-1	Trend fCO_2 µatm.yr^{-1}	Trend pH TS.decade^{-1}	Method
1963–2022	Apr–May	0.64 (0.20)	1.78 (0.13)	−0.019 (0.001)	Obs.
1960–1995	Annual	0.67 (0.05)	1.09 (0.05)	−0.012 (0.001)	Rec.
1995–2023	Annual	1.11 (0.08)	2.03 (0.07)	−0.020 (0.001)	Rec.
1960–1995	Annual	0.67 (0.05)	0.94 (0.05)	−0.010 (0.001)	no warming
1995–2023	Annual	1.11 (0.08)	1.84 (0.07)	−0.018 (0.001)	no warming
Warming effect	1960–1995		13.8 %	16.7 %	
Warming effect	1995–2023		9.4 %	10.0 %	

3.4. Air-sea CO_2 fluxes

The increasing of the CO_2 sink deduced from our results in the southern African coastal zone (here the MARCATS #25) is in line with previous data-based analysis in other shelves regions (Laruelle et al., 2018). This is also coherent with models results over 1998–2018 in this region (Resplandy et al., 2024; Mathis et al., 2024). Our recent observations in 2021–2022 also showed that the ocean CO_2 sink continued to increase (Fig. S7) that might be explained by lateral transport as suggested from modeling study (Roobaert et al., 2024).

The net flux of CO_2 across the air-sea interface (FCO_2) was calculated according to the following equation (5):

$$FCO_2 = k\ K0\ \Delta fCO_2 \quad (5)$$

Where $K0$ is the solubility of CO_2 in seawater calculated from in situ temperature and salinity (Weiss, 1974) and k (cm.h^{-1}) is the gas transfer velocity expressed from the wind speed U (m.s^{-1}) (Wanninkhof, 2014) and the Schmidt number Sc (Wanninkhof, 1992) following equation (6):

$$k = 0.251\ U^2\ (Sc/660)^{-0.5} \quad (6)$$

For the wind speed, we used the monthly values from MERRA-2 for 1980–2023 and the mean monthly values for years 1960–1979. In the coastal zone, winds are slightly higher than in the open ocean and in

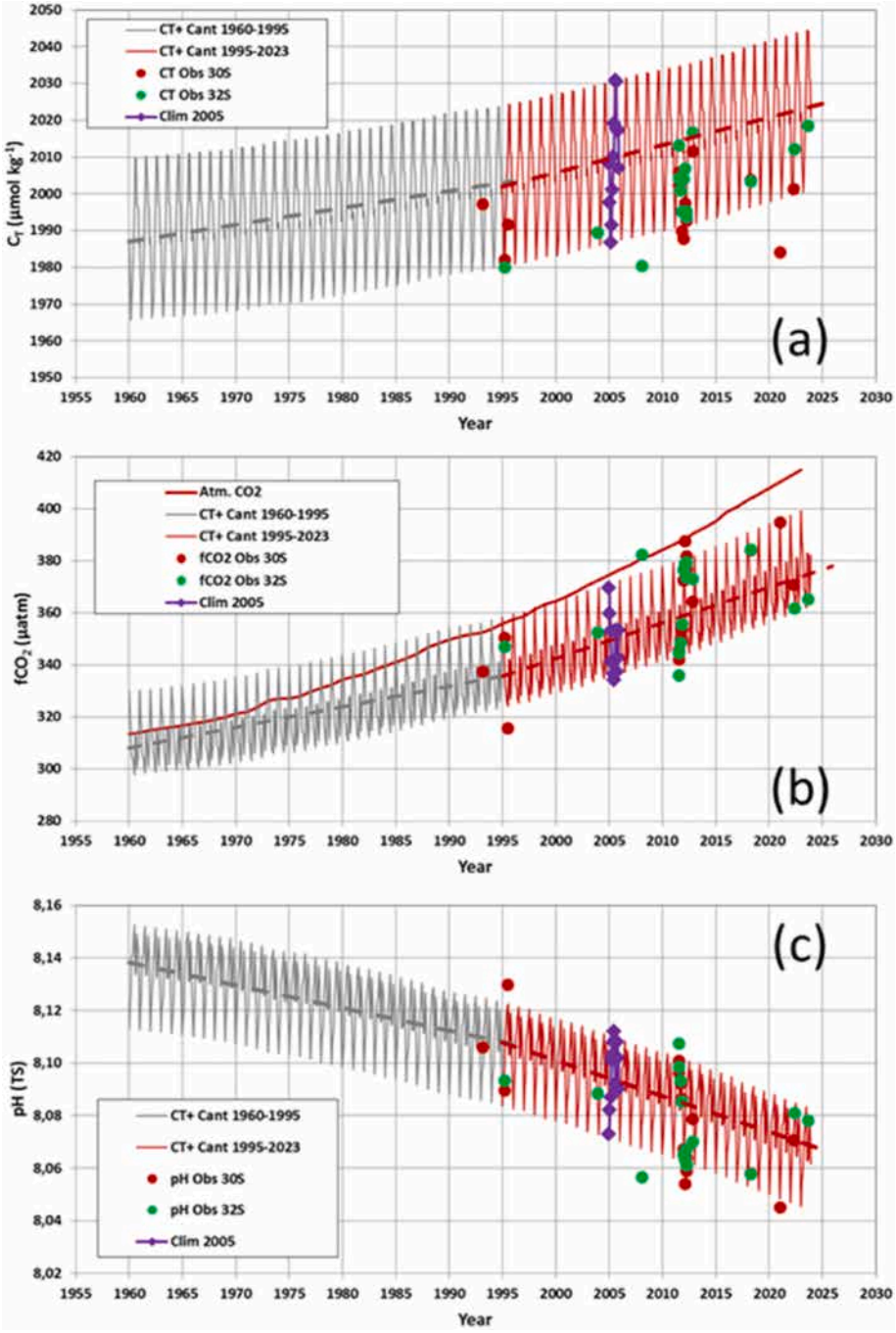

Fig. 9. Observed (red dots at 30°S for ADE, green dots at 32°S for ODE) and calculated time-series in the coastal region off Africa for (a) C_T (µmol.kg^{-1}), (b) fCO_2 (µatm) and (c) pH (TS). The lines show the evolution of the properties since 1960 corrected for C_{ant} where fCO_2, pH were recalculated using reconstructed C_T. Also shown the climatology for year 2005 (Purple diamonds, Takahashi et al., 2014). In (b) the red line is the atmospheric fCO_2. The trends (dashed line) are shown over 1960–1995 (grey) and 1995–2023 (red) (trends values are listed in Table 5).

Table 5
Trends of sea surface C_T (µmol.kg^{-1}.yr^{-1}), fCO_2 (µatm.yr^{-1}) and pH (TS.decade^{-1}) based on reconstruction method (Rec.) for different periods in the coastal region. See Fig. 9. Standard-deviations are given in brackets.

Period Period	Season	Trend C_T µmol.kg^{-1}.yr^{-1}	Trend fCO_2 µatm.yr^{-1}	Trend pH TS. decade^{-1}	Method
1960–1995	Annual	0.45 (0.06)	0.79 (0.04)	−0.0087 (0.0005)	Rec.
1995–2023	Annual	0.75 (0.09)	1.37 (0.07)	−0.014 (0.001)	Rec.

both regions no clear trend was detected for the wind since 1980 (Fig. S8). The long-term change of the CO_2 sink (Fig. 10) was mainly driven by ΔfCO_2 (Fig. S7). Inter-annual variability of the sink is observed during some periods such as in 2015 when the wind was relatively low in both regions but this has no effect on the trends. The trends of fluxes over 1960–2023 were −0.0238 ± 0.0001 molC/m^2/yr in the coastal zone and only −0.0058 ± 9.2 molC/m^2/yr in the Mozambique basin (Fig. 10). In the Mozambique basin the sink was −0.50 molC/m^2/yr in 1960 and increased to −0.77 molC/m^2/yr in 2022. In the coastal zone the sink was −0.13 molC/m^2/yr in 1960 and increased to −1.52 molC/m^2/yr in 2022 (Table 6). Over 2005–2012 we estimated an average sink

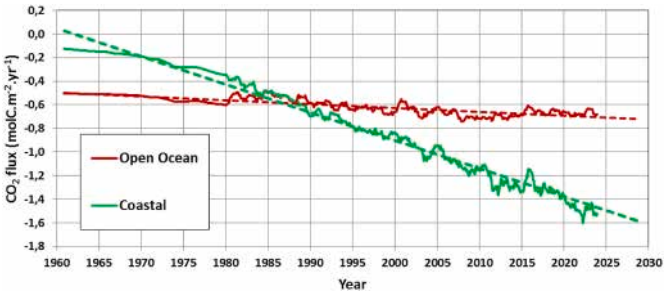

Fig. 10. Reconstructed time-series of the CO_2 fluxes (molC.m^{-2}.yr^{-1}) in the Mozambique Basin (open ocean region, red) and in the African coastal zone (green). Corresponding linear trends are indicated in dashed.

of -1.16 ± 0.08 molC/m^2/yr in the coastal zone that is 30% lower than -1.65 ± 0.04 molC/m^2/yr previously reported by Arnone et al. (2017) based on fCO_2 observations for the same period (Table 6). Compared to ocean models (Bourgeois et al., 2016), our reconstructed results in the Agulhas coastal zone (region MARCATS #25) for 1990–2011 (-0.93 ± 0.17 molC/m^2/yr) are in the same range but stronger than deduced from data-based product for the same period (Laruelle et al., 2014, Table 6). The CO_2 flux deduced from observations in 1963–2023 showed a clear seasonality (Fig. S9a) but there are not enough observations each year to integrate annual values (Fig. S9b). This is why the fluxes deduced from observations are presented in mmolC/m^2/d^{-1} (Table 6). However, they confirmed that both regions were acting as an ocean CO_2 sink except in the Mozambique basin in December 2003/January 2004 (Table 6, Fig. S9b) when the region was warmer (Fig. S4).

4. Summary and concluding remarks

The observations obtained in January 2021 and May 2022 presented in this study offered a new description of the spatial and temporal variability of the carbonate system in the South Western Indian Ocean, the Agulhas Current system and near the African coast. For the seasonal cycle, the new data in May 2022 complemented previous cruises conducted in January–April and June–December (Bakker et al., 2016, 2024). In the Mozambique Basin the fCO_2 distribution was rather homogeneous in January and May with some lower fCO_2 and C_T concentrations localized south of Madagascar associated to productive areas probably linked to diazotrophy. In this region the ocean was a small CO_2 sink in January 2021 (-0.5 mmolC.m^{-2}.d^{-1}) and much stronger in May 2022 during a colder season (-2.4 mmolC.m^{-2}.d^{-1}). In the Agulhas Current system and near the African coast the variability of fCO_2 was very large with ΔfCO_2 ranging between -20 and -80 µatm in May 2022. Based on observations we estimated that the coastal zone was a strong sink in May 2022 (-4.3 mmolC.m^{-2}.d^{-1}). To explore the trends and the drivers of the ocean carbonate system at decadal scale, we separated the domain following two regions, the Mozambique Basin and the coastal areas. Using sea surface fCO_2 data available since 1995 we found a faster fCO_2 increase in the Mozambique Basin (2.03 ± 0.07 µatm.yr^{-1}) compared to the coastal zone (1.37 ± 0.07 µatm.yr^{-1}). From the water column data obtained between 1987 and 2021, we estimated positive trends of the anthropogenic CO_2 concentrations in subsurface that enabled to reconstruct the temporal changes of the carbonate system since 1960. The reconstructed air-sea CO_2 fluxes indicate that the oceanic CO_2 sink increased over time, a change that was more pronounced in the coastal zone. The accumulation of anthropogenic CO_2 droved the continuous increase of fCO_2 and C_T and the decrease of pH. In the Mozambique Basin, the lowest pH (8.039) was observed in January 2021. It was higher in May 2022 (8.062) and lower by -0.106 than observed 59 years ago for the same season (May 1963); this is close to the difference of -0.11 estimated on average for the global ocean since the pre-industrial era (Jiang et al., 2019). In the coastal zone the lowest pH (8.045) was also observed in January 2021 and highly variable in May 2022 with values ranging between 8.05 and 8.11. In both regions, the pH decrease was about twice faster in the last 3 decades (1995–2023). The pH trend was faster in the open ocean (-0.020 ± 0.001.decade^{-1}) compared to the coastal zones (-0.014 ± 0.001.

Table 6
Air-sea CO_2 fluxes estimated in the investigated region from different methods and for different periods (negative values represent an ocean CO_2 sink). Annual fluxes are expressed in molC/m^2/yr; observational fluxes for the OISO-31 cruise in January 2021 and RESILIENCE cruise in May 2022 expressed in molC/m^2/d. Standard-deviations are given in brackets. For the methods, the results based on reconstruction noted Rec. and from observations noted Obs.

Region		Flux molC.m-2.yr-1	Method	Year/Period	Ref
Open Ocean	37.5°E–32°S	−0.66	Climatology	2000	Takahashi et al. (2009)
Open Ocean	37.5°E–32°S	−1.04	Climatology	2010	Fay et al. (2024)
Open Ocean	32.5°E–32°S	−1.13	Climatology	2000	Takahashi et al. (2009)
Open Ocean	32.5°E–32°S	−1.70	Climatology	2010	Fay et al. (2024)
Coastal Zone	30°E–32°S	−1.65 (0.04)	Observations	2005–2012	Arnone et al. (2017)
Coastal Zone	MARCATS #25	−0.58	Data-Based	1990–2011	Laruelle et al. (2014)
Coastal Zone	MARCATS #25	−1.20 (0.09)	Model	1990–2011	Bourgeois et al. (2016)
Open Ocean	Mozambique	−0.74	Rec.	2000	This study
Open Ocean	Mozambique	−0.80	Rec.	2010	This study
Coastal Zone	30°S	−1.16	Rec.	2010	This study
Coastal Zone	30°S	−1.16 (0.08)	Rec.	2005–2012	This study
Coastal Zone	30°S	−0.93 (0.17)	Rec.	1990–2011	This study
Open Ocean	Mozambique	−0.50	Rec.	1960	This study
Open Ocean	Mozambique	−0.77	Rec.	2022	This study
Coastal Zone	30°S	−0.13	Rec.	1960	This study
Coastal Zone	30°S	−1.52	Rec.	2022	This study
Region		Flux mmolC/m^2/d	Method	Year/Period	Ref
Open Ocean	Mozambique	−2.39	Rec.	May 2022	This study
Coastal Zone	30°S	−3.38	Rec.	May 2022	This study
Open Ocean	Mozambique	+0.87	Obs.	Jan 2004	This study
Open Ocean	Mozambique	−0.46	Obs.	Jan 2021	This study
Open Ocean	Mozambique	−2.37	Obs.	May 2022	This study
Coastal Zone	30°S	−3.51	Obs.	May 2022	This study
Coastal Zone	32°S	−4.30	Obs.	May 2022	This study

decade^{-1}). The rate of OA deduced from our reconstruction is low compared to the first estimate in the Indian Ocean Subtropics for the period 1991–2011 (-0.027 ± 0.01.decade^{-1}, Lauvset et al., 2015) but in the range of recent neural network data-based method (-0.018 ± 0.001.decade^{-1}, Chau et al., 2024). Although there are relatively few data available at different seasons and years, our recent observations confirmed the acidification deduced from the reconstruction (Figs. 8 and 9). In austral summer the observed pH in the coastal zone changed from 8.106 in February 1993 to 8.045 in January 2021. In austral autumn, observed pH changed from 8.130 in June 1995 to 8.070 May 2022. The decrease of pH was mainly driven by anthropogenic CO_2 uptake and also linked to the long term warming that represents about 10% of the pH changes.

Given the high variability of the carbonate system in the Agulhas Current system and in the coastal zone (here the MARCATS #25 region) more observations and dedicated models are needed to better evaluate and understand the processes that control the air-sea CO_2 fluxes and ocean acidification in such dynamics region, as well as the impact of chemistry change on the marine ecosystem in the future. Our present study based on fCO_2, A_T and C_T data calls for detailed analyses that couple chemical and biological observations, such as dinitrogen fixation that present high rates near the South African coast and in the South Western Indian Ocean (Chowdhury et al., 2024). Our analysis was dedicated to evaluate changes of the carbonate system in surface waters. In subsurface, we estimated C_{ant} concentrations close to 60 μmol kg^{-1} in 2021, a signal identified down to 500m. This should be investigated with new observations in the future as it has been recently recognized that this region present significant decadal differences of the C_{ant} inventories (Müller et al., 2023), a signal that should be revisited to estimate the transport of C_{ant} from the Indian Ocean towards the South Atlantic Ocean through the Agulhas Current and associated eddies or transported back to the Southern Indian Ocean through the Agulhas Return Current (Lo Monaco et al., 2005; Evans et al., 2017; Orselli et al., 2019).

CRediT authorship contribution statement

Nicolas Metzl: Writing – original draft, Methodology, Funding acquisition, Formal analysis, Data curation, Conceptualization. **Claire Lo Monaco:** Investigation, Funding acquisition, Data curation. **Guillaume Barut:** Formal analysis. **Jean-François Ternon:** Writing – review & editing, Funding acquisition, Conceptualization.

Declaration of competing interest

The authors declare that they have no known competing financial interests or personal relationships that could have appeared to influence the work reported in this paper.

Acknowledgment

The OISO program was supported by the French institutes INSU (Institut National des Sciences de l'Univers) and IPEV (Institut Polaire Paul-Emile Victor), OSU Ecce-Terra (at Sorbonne Université), the French programs SOERE/Great-Gases and ICOS-France. We thank the French Oceanographic Fleet for financial and logistic support for the OISO program (https://campagnes.flotteoceanographique.fr/series/228/). The RESILIENCE cruise (https://doi.org/10.17600/18001917) was supported by the French National Oceanographic Fleet, by the Belmont Forum Ocean Front Change project, by the ISblue project and by the French National program LEFE (Les Enveloppes Fluides et l'Environnement). We thank the captains and crew of R.R.V. Marion-Dufresne and the staff at IFREMER, GENAVIR and IPEV. We also thank Jonathan Fin and Claude Mignon at LOCEAN laboratory for their help during the OISO and RESILIENCE cruises. We thank all colleagues that contributed to the quality control of ocean data made available through GLODAP (www.glodap.info). The Surface Ocean CO_2 Atlas (SOCAT, www.socat.info) is an international effort, endorsed by the International Ocean Carbon Coordination Project (IOCCP), the Surface Ocean Lower Atmosphere Study (SOLAS) and the Integrated Marine Biogeochemistry and Ecosystem Research program (IMBER), to deliver a uniformly quality-controlled surface ocean CO_2 database. We thank the two anonymous reviewers for making constructive suggestions, which resulted in improvements of this paper and Raleigh Hood, Editor of this IIOE-2 special issue.

Appendix A. Supplementary data

Supplementary data to this article can be found online at https://doi.org/10.1016/j.dsr2.2025.105459.

Data availability

All data, including new data, used are available in public data-bases (SOCAT, GLODAP, NCEI/OCADS)

References

Antonov, J.I., Locarnini, R.A., Boyer, T.P., Mishonov, A.V., Garcia, H.E., 2006. World Ocean Atlas 2005. In: Levitus, S. (Ed.), Volume 2: Salinity, NOAA Atlas NESDIS 62. US Government Printing Office, Washington, DC, p. 182.

Arnone, V., González-Dávila, M., Magdalena Santana-Casiano, J., 2017. CO2 fluxes in the South African coastal region. Mar. Chem. 195, 41–49. https://doi.org/10.1016/j.marchem.2017.07.008.

Bakker, D.C.E., Pfeil, B., Landa, C.S., Metzl, N., O'Brien, K.M., Olsen, A., Smith, K., Cosca, C., Harasawa, S., Jones, S.D., Nakaoka, S.-I., Nojiri, Y., Schuster, U., Steinhoff, T., Sweeney, C., Takahashi, T., Tilbrook, B., Wada, C., Wanninkhof, R., Alin, S.R., Balestrini, C.F., Barbero, L., Bates, N.R., Bianchi, A.A., Bonou, F., Boutin, J., Bozec, Y., Burger, E.F., Cai, W.-J., Castle, R.D., Chen, L., Chierici, M., Currie, K., Evans, W., Featherstone, C., Feely, R.A., Fransson, A., Goyet, C., Greenwood, N., Gregor, L., Hankin, S., Hardman-Mountford, N.J., Harlay, J., Hauck, J., Hoppema, M., Humphreys, M.P., Hunt, C.W., Huss, B., Ibánhez, J.S.P., Johannessen, T., Keeling, R., Kitidis, V., Körtzinger, A., Kozyr, A., Krasakopoulou, E., Kuwata, A., Landschützer, P., Lauvset, S.K., Lefèvre, N., Lo Monaco, C., Manke, A., Mathis, J.T., Merlivat, L., Millero, F.J., Monteiro, P.M.S., Munro, D.R., Murata, A., Newberger, T., Omar, A.M., Ono, T., Paterson, K., Pearce, D., Pierrot, D., Robbins, L. L., Saito, S., Salisbury, J., Schlitzer, R., Schneider, B., Schweitzer, R., Sieger, R., Skjelvan, I., Sullivan, K.F., Sutherland, S.C., Sutton, A.J., Tadokoro, K., Telszewski, M., Tuma, M., Van Heuven, S.M.A.C., Vandemark, D., Ward, B., Watson, A.J., Xu, S., 2016. A multi-decade record of high-quality fCO_2 data in version 3 of the Surface Ocean CO_2 Atlas (SOCAT). Earth Syst. Sci. Data 8, 383–413. https://doi.org/10.5194/essd-8-383-2016.

Bakker, Dorothee C.E., Alin, Simone R., Bates, Nicholas, Becker, Meike, Gkritzalis, Thanos, Jones, Steve D., Kozyr, Alex, Lauvset, Siv K., Metzl, Nicolas, Nakaoka, Shin-ichiro, O'Brien, Kevin M., Olsen, Are, Pierrot, Denis, Steinhoff, Tobias, Sutton, Adrienne J., Takao, Shintaro, Tilbrook, Bronte, Wada, Chisato, Wanninkhof, Rik, Akl, John, Arbilla, Lisandro A., Arruda, Ricardo, Azetsu-Scott, Kumiko, Barbero, Leticia, Beatty, Cory M., Berghoff, Carla F., Bittig, Henry C., Burger, Eugene F., Campbell, Katie, Cardin, Vanessa, Collins, Andrew, Coppola, Laurent, Cronin, Margot, Cross, Jessica N., Currie, Kim I., Emerson, Steven R., Enright, Matt P., Enyo, Kazutaka, Evans, Wiley, Feely, Richard A., Flohr, Anita, Gehrung, Martina, Glockzin, Michael, González-Dávila, Melchor, Hamnca, Siyabulela, Hartman, Sue, Howden, Stephan D., Kam, Kitty, Kamb, Linus, Körtzinger, Arne, Kosugi, Naohiro, Lefèvre, Nathalie, Lo Monaco, Claire, Macovei, Vlad A., Maenner Jones, Stacy, Manalang, Dana, Martz, Todd R., Mdokwana, Baxolele, Monacci, Natalie M., Monteiro, Pedro M.S., Mordy, Calvin, Morell, Julio M., Murata, Akihiko, Neill, Craig, Noh, Jae-Hoon, Nojiri, Yukihiro, Ohman, Mark, Olivier, Léa, Ono, Tsuneo, Petersen, Wilhelm, Plueddemann, Albert J., Prytherch, John, Rehder, Gregor, Rutgersson, Anna, Santana-Casiano, J. Magdalena, Schlitzer, Reiner, Send, Uwe, Skjelvan, Ingunn, Sullivan, Kevin F., T'Jampens, Michiel, Tadokoro, Kazuaki, Telszewski, Maciej, Theetaert, Hannelore, Tsanwani, Mutshutshu, Vandemark, Douglas, van Ooijen, Erik, Veccia, Martín H., Voynova, Yoana G., Wang, Hongjie, Weller, Robert A., Woosley, Ryan J., 2024. Surface Ocean CO2 Atlas Database Version 2024 (SOCATv2024) (NCEI Accession 0293257). NOAA National Centers for Environmental Information. Dataset. https://doi.org/10.25921/9wpn-th28. (Accessed 30 June 2024).

Bourgeois, T., Orr, J.C., Resplandy, L., Terhaar, J., Ethé, C., Gehlen, M., Bopp, L., 2016. Coastal-ocean uptake of anthropogenic carbon. Biogeosciences 13, 4167–4185. https://doi.org/10.5194/bg-13-4167-2016.

Chakraborty, K., Joshi, A.P., Ghoshaln, P.K., Baduru, B., Valsala, V., Sarma, V.V.S.S., Metzl, N., Gehlen, M., Chevallier, F., Lo Monaco, C., 2024. Indian Ocean acidification and its driving mechanisms over the last four decades (1980-2019). Global Biogeochem. Cycles 38, e2024GB008139. https://doi.org/10.1029/2024GB008139.

Chau, T.-T.-T., Gehlen, M., Metzl, N., Chevallier, F., 2024. CMEMS-LSCE: a global, 0.25°, monthly reconstruction of the surface ocean carbonate system. Earth Syst. Sci. Data 16, 121–160. https://doi.org/10.5194/essd-16-121-2024.

Cheng, L.J., Abraham, J., Zhu, J., Trenberth, K.E., Fasullo, J., Boyer, T., Locarnini, R., Zhang, B., Yu, F.J., Wan, L.Y., Chen, X.R., Song, X.Z., Liu, Y.L., Mann, M.E., 2020. Record-setting ocean warmth continued in 2019. Adv. Atmos. Sci. 37, 137–142. https://doi.org/10.1007/s00376-020-9283-7.

Cheng, L., Abraham, J., Trenberth, K.E., et al., 2024. New record ocean temperatures and related climate indicators in 2023. Adv. Atmos. Sci. https://doi.org/10.1007/s00376-024-3378-5.

Chowdhury, S., Berthelot, H., Baudet, C., et al., 2024. Fronts divide diazotroph communities in the Southern Indian Ocean. FEMS (Fed. Eur. Microbiol. Soc.) Microbiol. Ecol. 2024, 100. https://doi.org/10.1093/femsec/fiae095.

Copin-Montégut, C., 1988. A new formula for the effect of temperature on the partial pressure of CO2 in seawater. Mar. Chem. 25, 29–37. https://doi.org/10.1016/0304-4203(88)90012-6.

Copin-Montégut, C., 1989. A new formula for the effect of temperature on the partial pressure of CO2 in seawater. Corrigendum. Mar. Chem. 27, 143–144. https://doi.org/10.1016/0304-4203(89)90034-0.

De Vries, T., Yamamoto, K., Wanninkhof, R., Gruber, N., Hauck, J., Müller, J.D., et al., 2023. Magnitude, trends, and variability of the global ocean carbon sink from 1985-2018. Glob. Biogeochem. Cycles 37, e2023GB007780. https://doi.org/10.1029/2023GB007780.

Dickson, A.G., 1990. Standard potential of the reaction: AgCl(s) + ½H2(g) = Ag(s) + HCl (aq), and the standard acidity constant of the ion HSO4– in synthetic sea water from 273.15 to 318.15 K. J. Chem. Thermodyn. 22, 113–127. https://doi.org/10.1016/0021-9614(90)90074-Z.

Doney, S.C., Busch, D.S., Cooley, S.R., Kroeker, K.J., 2020. The impacts of ocean acidification on marine ecosystems and reliant human communities. Annu. Rev. Environ. Resour. 45 (1). https://doi.org/10.1146/annurev-environ-012320-083019.

Doney, S.C., Fabry, V.J., Feely, R.A., Kleypas, J.A., 2009. Ocean acidification: The other CO2 problem. Annu. Rev. Mar. Sci. 1 (1), 169–192. https://doi.org/10.1146/annurev.marine.010908.163834.

Edmond, J.M., 1970. High precision determination of titration alkalinity and total carbon dioxide content of sea water by potentiometric titration. Deep-Sea Res. 17, 737–750. https://doi.org/10.1016/0011-7471(70)90038-0.

Evans, G.R., McDonagh, E.L., King, B.A., Bryden, H.L., Bakker, D.C.E., Brown, P.J., Schuster, U., Speer, K.G., van Heuven, S.M.A.C., 2017. South Atlantic interbasin exchanges of mass, heat, salt and anthropogenic carbon. Prog. Oceanogr. 151, 62–82. https://doi.org/10.1016/j.pocean.2016.11.005.

Fabry, V.J., Seibel, B.A., Feely, R.A., Orr, J.C., 2008. Impacts of ocean acidification on marine fauna and ecosystem processes. ICES J. Mar. Sci. 65, 414–432. https://doi.org/10.1093/icesjms/fsn048.

Fay, A.R., Munro, D.R., McKinley, G.A., Pierrot, D., Sutherland, S.C., Sweeney, C., Wanninkhof, R., 2024. Updated climatological mean ΔfCO2 and net sea–air CO2 flux over the global open ocean regions. Earth Syst. Sci. Data 16, 2123–2139. https://doi.org/10.5194/essd-16-2123-2024.

Fontela, M., Vélo, A., Gilcoto, M., Pérez, F., 2021. Anthropogenic CO2 and Ocean Acidification in Argentine basin water masses over almost five decades of observations. Sci. Total Environ. 779. https://doi.org/10.1016/j.scitotenv.2021.146570.

Friedlingstein, P., O'Sullivan, M., Jones, M.W., Andrew, R.M., Bakker, D.C.E., Hauck, J., Landschützer, P., Le Quéré, C., Luijkx, I.T., Peters, G.P., Peters, W., Pongratz, J., Schwingshackl, C., Sitch, S., Canadell, J.G., Ciais, P., Jackson, R.B., Alin, S.R., Anthoni, P., Barbero, L., Bates, N.R., Becker, M., Bellouin, N., Decharme, B., Bopp, L., Brasika, I.B.M., Cadule, P., Chamberlain, M.A., Chandra, N., Chau, T.-T.-T., Chevallier, F., Chini, L.P., Cronin, M., Dou, X., Enyo, K., Evans, W., Falk, S., Feely, R. A., Feng, L., Ford, D.J., Gasser, T., Ghattas, J., Gkritzalis, T., Grassi, G., Gregor, L., Gruber, N., Gürses, Ö., Harris, I., Hefner, M., Heinke, J., Houghton, R.A., Hurtt, G.C., Iida, Y., Ilyina, T., Jacobson, A.R., Jain, A., Jarníková, T., Jersild, A., Jiang, F., Jin, Z., Joos, F., Kato, E., Keeling, R.F., Kennedy, D., Klein Goldewijk, K., Knauer, J., Korsbakken, J.I., Körtzinger, A., Lan, X., Lefèvre, N., Li, H., Liu, J., Liu, Z., Ma, L., Marland, G., Mayot, N., McGuire, P.C., McKinley, G.A., Meyer, G., Morgan, E.J., Munro, D.R., Nakaoka, S.-I., Niwa, Y., O'Brien, K.M., Olsen, A., Omar, A.M., Ono, T., Paulsen, M., Pierrot, D., Pocock, K., Poulter, B., Powis, C.M., Rehder, G., Resplandy, L., Robertson, E., Rödenbeck, C., Rosan, T.M., Schwinger, J., Séférian, R., Smallman, T.L., Smith, S.M., Sospedra-Alfonso, R., Sun, Q., Sutton, A.J., Sweeney, C., Takao, S., Tans, P.P., Tian, H., Tilbrook, B., Tsujino, H., Tubiello, F., van der Werf, G. R., van Ooijen, E., Wanninkhof, R., Watanabe, M., Wimart-Rousseau, C., Yang, D., Yang, X., Yuan, W., Yue, X., Zaehle, S., Zeng, J., Zheng, B., 2023. Global Carbon Budget 2023. Earth Syst. Sci. Data 15, 5301–5369. https://doi.org/10.5194/essd-15-5301-2023.

Friedlingstein, P., O'Sullivan, M., Jones, M.W., Andrew, R.M., Gregor, L., Hauck, J., Le Quéré, C., Luijkx, I.T., Olsen, A., Peters, G.P., Peters, W., Pongratz, J., Schwingshackl, C., Sitch, S., Canadell, J.G., Ciais, P., Jackson, R.B., Alin, S.R., Alkama, R., Arneth, A., Arora, V.K., Bates, N.R., Becker, M., Bellouin, N., Bittig, H.C., Bopp, L., Chevallier, F., Chini, L.P., Cronin, M., Evans, W., Falk, S., Feely, R.A., Gasser, T., Gehlen, M., Gkritzalis, T., Gloege, L., Grassi, G., Gruber, N., Gürses, Ö., Harris, I., Hefner, M., Houghton, R.A., Hurtt, G.C., Iida, Y., Ilyina, T., Jain, A.K., Jersild, A., Kadono, K., Kato, E., Kennedy, D., Klein Goldewijk, K., Knauer, J., Korsbakken, J.I., Landschützer, P., Lefèvre, N., Lindsay, K., Liu, J., Liu, Z., Marland, G., Mayot, N., McGrath, M.J., Metzl, N., Monacci, N.M., Munro, D.R., Nakaoka, S.-I., Niwa, Y., O'Brien, K., Ono, T., Palmer, P.I., Pan, N., Pierrot, D., Pocock, K., Poulter, B., Resplandy, L., Robertson, E., Rödenbeck, C., Rodriguez, C., Rosan, T.M., Schwinger, J., Séférian, R., Shutler, J.D., Skjelvan, I., Steinhoff, T., Sun, Q., Sutton, A.J., Sweeney, C., Takao, S., Tanhua, T., Tans, P.P., Tian, X., Tian, H., Tilbrook, B., Tsujino, H., Tubiello, F., van der Werf, G.R., Walker, A.P., Wanninkhof, R., Whitehead, C., Willstrand Wranne, A., Wright, R., Yuan, W., Yue, C., Yue, X., Zaehle, S., Zeng, J., Zheng, B., 2022. Global Carbon Budget 2022. Earth Syst. Sci. Data 14, 4811–4900. https://doi.org/10.5194/essd-14-4811-2022.

Ghosh, J., Chakraborty, K., Valsala, V., Bhattacharya, T., Ghoshal, P.K., 2024. A review of the Indian Ocean carbon dynamics, acidity, and productivity in a changing environment. Prog. Oceanogr. 221, 103210. https://doi.org/10.1016/j.pocean.2024.103210.

González-Dávila, M., Santana Casiano, J.M., Machín, F., 2017. Changes in the partial pressure of carbon dioxide in the Mauritanian–Cap Vert upwelling region between 2005 and 2012. Biogeosciences 14, 3859–3871. https://doi.org/10.5194/bg-14-3859-2017.

Guastella, L.A., Roberts, M.J., 2016. Dynamics and role of the Durban cyclonic eddy in the KwaZulu-Natal Bight ecosystem. Afr. J. Mar. Sci. 38 (Suppl. ment), S23–S42. https://doi.org/10.2989/1814232X.2016.1159982.

Jiang, L.-Q., Carter, B.R., Feely, R.A., Lauvset, S.K., Olsen, A., 2019. Surface ocean pH and buffer capacity: past, present and future. Sci. Rep. 9 (1), 1–11. https://doi.org/10.1038/s41598-019-55039-4.

Jiang, L.-Q., Dunne, J., Carter, B.R., Tjiputra, J.F., Terhaar, J., Sharp, J.D., et al., 2023. Global surface ocean acidification indicators from 1750 to 2100. J. Adv. Model. Earth Syst. 15, e2022MS003563. https://doi.org/10.1029/2022MS003563.

Keeling, C.D., Waterman, L.S., 1968. Carbon dioxide in surface ocean waters: 3. Measurements on Lusiad Expedition 1962–1963. J. Geophys. Res. 73 (14), 4529–4541. https://doi.org/10.1029/JB073i014p04529.

Kwiatkowski, L., Torres, O., Bopp, L., Aumont, O., Chamberlain, M., Christian, J.R., Dunne, J.P., Gehlen, M., Ilyina, T., John, J.G., Lenton, A., Li, H., Lovenduski, N.S., Orr, J.C., Palmieri, J., Santana-Falcón, Y., Schwinger, J., Séférian, R., Stock, C.A., Tagliabue, A., Takano, Y., Tjiputra, J., Toyama, K., Tsujino, H., Watanabe, M., Yamamoto, A., Yool, A., Ziehn, T., 2020. Twenty-first century ocean warming, acidification, deoxygenation, and upper-ocean nutrient and primary production decline from CMIP6 model projections. Biogeosciences 17, 3439–3470. https://doi.org/10.5194/bg-17-3439-2020.

Laruelle, G.G., Dürr, H.H., Lauerwald, R., Hartmann, J., Slomp, C.P., Goossens, N., Regnier, P.A.G., 2013. Global multi-scale segmentation of continental and coastal waters from the watersheds to the continental margins. Hydrol. Earth Syst. Sci. 17, 2029–2051. https://doi.org/10.5194/hess-17-2029-2013.

Laruelle, G.G., Lauerwald, R., Pfeil, B., Regnier, P., 2014. Regionalized global budget of the CO2 exchange at the air-water interface in continental shelf seas. Global Biogeochem. Cy. 28, 1199–1214. https://doi.org/10.1002/2014GB004832.

Laruelle, G.G., Cai, W.-J., Hu, X., Gruber, N., Mackenzie, F.T., Regnier, P., 2018. Continental shelves as a variable but increasing global sink for atmospheric carbon dioxide. Nat. Commun. 9, 454. https://doi.org/10.1038/s41467-017-02738-z.

Lauvset, S.K., Gruber, N., Landschützer, P., Olsen, A., Tjiputra, J., 2015. Trends and drivers in global surface ocean pH over the past 3 decades. Biogeosciences 12, 1285–1298. https://doi.org/10.5194/bg-12-1285-2015.

Lauvset, S.K., Lange, N., Tanhua, T., Bittig, H.C., Olsen, A., Kozyr, A., Álvarez, M., Azetsu-Scott, K., Brown, P.J., Carter, B.R., Cotrim da Cunha, L., Hoppema, M., Humphreys, M.P., Ishii, M., Jeansson, E., Murata, A., Müller, J.D., Pérez, F.F., Schirnick, C., Steinfeldt, R., Suzuki, T., Ulfsbo, A., Velo, A., Woosley, R.J., Key, R.M., 2024. The annual update GLODAPv2.2023: the global interior ocean biogeochemical data product. Earth Syst. Sci. Data 16, 2047–2072. https://doi.org/10.5194/essd-16-2047-2024.

Lewis, E., Wallace, D.W.R., 1998. Program developed for CO2 system calculations. ORNL/CDIAC-105. Carbon Dioxide Information Analysis Center. Oak Ridge National Laboratory, US. Dept. of Energy, Oak Ridge, TN. https://doi.org/10.2172/639712.

Lo Monaco, C., Metzl, N., Fin, J., Mignon, C., Cuet, P., Douville, E., Gehlen, M., Trang Chau, T.T., Tribollet, A., 2021. Distribution and long-term change of the sea surface carbonate system in the Mozambique Channel. Deep-Sea Res. Part II. https://doi.org/10.1016/j.dsr2.2021.104936, 1963-2019.

Lo Monaco, C., Metzl, N., Fin, J., 2023. Sea surface measurements of dissolved inorganic carbon (DIC). Total Alkalinity (TALK), Temperature and Salinity during the R/V Marion-Dufresne Ocean Indien Service d'Observations - 31 (OISO-31) Cruise (EXPOCODE 35MV20210113) in the Indian Ocean from 2021-01-14 to 2021-03-04 (NCEI Accession 0280946. NOAA National Centers for Environmental Information. Dataset. https://doi.org/10.25921/7sb2-k852. (Accessed 30 June 2024).

Lo Monaco, C., Metzl, N., 2024. Surface Underway Measurements of Partial Pressure of Carbon Dioxide (pCO2), Salinity, Water Temperature and Other Associated Parameters during the R/V Marion Dufresne RESILIENCE Cruise (EXPOCODE 35MV20220420) in the Indian Ocean from 2022-04-20 to 2022-05-21 (NCEI Accession 0287480). NOAA National Centers for Environmental Information. Dataset. https://doi.org/10.25921/zqbp-bw28. (Accessed 30 June 2024).

Lo Monaco, C., Metzl, N., Poisson, A., Brunet, C., Schauer, B., 2005. Anthropogenic CO2 in the Southern Ocean: distribution and inventory at the Indo-Atlantic boundary (WOCE line I6). J. Geophys. Res. 110, C06010. https://doi.org/10.1029/2004JC002643.

Lueker, T.J., Dickson, A.G., Keeling, C.D., 2000. Ocean pCO(2) calculated from dissolved inorganic carbon, alkalinity, and equations for K-1 and K-2: validation based on laboratory measurements of CO2 in gas and seawater at equilibrium. Mar. Chem. 70, 105–119. https://doi.org/10.1016/S0304-4203(00)00022-0.

Madkaiker, K., Valsala, V., Sreeush, M.G., Mallissery, A., Chakraborty, K., Deshpande, A., 2023. Understanding the seasonality, trends, and controlling factors of Indian Ocean acidification over distinctive bio-provinces. J. Geophys. Res.: Biogeosciences 128, e2022JG006926. https://doi.org/10.1029/2022JG006926.

Mathis, M., Lacroix, F., Hagemann, S., et al., 2024. Enhanced CO2 uptake of the coastal ocean is dominated by biological carbon fixation. Nat. Clim. Chang. https://doi.org/10.1038/s41558-024-01956-w.

Metzl, N., Louanchi, F., Poisson, A., 1998. Seasonal and interannual variations of sea surface carbon dioxide in the subtropical indian ocean. Mar. Chem. 60, 131–146. https://doi.org/10.1016/S0304-4203(98)00083-8.

Metzl, N., Lo Monaco, C., Leseurre, C., Ridame, C., Fin, J., Mignon, C., Gehlen, M., Chau, T.T.T., 2022. The impact of the South-East Madagascar Bloom on the oceanic CO2 sink. Biogeosciences 19, 1451–1468. https://doi.org/10.5194/bg-19-1451-2022.

Millero, F.J., Lee, K., Roche, M., 1998. Distribution of alkalinity in the surface waters of the major oceans. Mar. Chem. 60, 111–130. https://doi.org/10.1016/S0304-4203(97)00084-4.

Müller, J.D., Gruber, N., Carter, B., Feely, R., Ishii, M., Lange, N., et al., 2023. Decadal trends in the oceanic storage of anthropogenic carbon from 1994 to 2014. AGU Advances 4, e2023AV000875. https://doi.org/10.1029/2023AV000875.

Murata, A., Kumamoto, Y., Sasaki, K., Watanabe, S., Fukasawa, M., 2010. Decadal increases in anthropogenic CO2 along 20°S in the SouthSouth Indian ocean. J. Geophys. Res. 115, C12055. https://doi.org/10.1029/2010JC006250.

Orr, J.C., Epitalon, J.-M., Dickson, A.G., Gattuso, J.-P., 2018. Routine uncertainty propagation for the marine carbon dioxide system. Mar. Chem. 207, 84–107. https://doi.org/10.1016/j.marchem.2018.10.006.

Orselli, I.B.M., Goyet, C., Kerr, R., de Azevedo, J.L.L., Araujo, M., Galdino, F., Touratier, F., Garcia, C.A.E., 2019. The effect of Agulhas eddies on absorption and transport of anthropogenic carbon in the South Atlantic Ocean. Climate 7 (6), 84. https://doi.org/10.3390/cli7060084.

Pfeil, B., Olsen, A., Bakker, D.C.E., Hankin, S., Koyuk, H., Kozyr, A., Malczyk, J., Manke, A., Metzl, N., Sabine, C.L., Akl, J., Alin, S.R., Bates, N., Bellerby, R.G.J., Borges, A., Boutin, J., Brown, P.J., Cai, W.-J., Chavez, F.P., Chen, A., Cosca, C., Fassbender, A.J., Feely, R.A., González-Dávila, M., Goyet, C., Hales, B., Hardman-Mountford, N., Heinze, C., Hood, M., Hoppema, M., Hunt, C.W., Hydes, D., Ishii, M., Johannessen, T., Jones, S.D., Key, R.M., Körtzinger, A., Landschützer, P., Lauvset, S. K., Lefèvre, N., Lenton, A., Lourantou, A., Merlivat, L., Midorikawa, T., Mintrop, L., Miyazaki, C., Murata, A., Nakadate, A., Nakano, Y., Nakaoka, S., Nojiri, Y., Omar, A. M., Padin, X.A., Park, G.-H., Paterson, K., Perez, F.F., Pierrot, D., Poisson, A., Ríos, A. F., Santana-Casiano, J.M., Salisbury, J., Sarma, V.V.S.S., Schlitzer, R., Schneider, B., Schuster, U., Sieger, R., Skjelvan, I., Steinhoff, T., Suzuki, T., Takahashi, T., Tedesco, K., Telszewski, M., Thomas, H., Tilbrook, B., Tjiputra, J., Vandemark, D., Veness, T., Wanninkhof, R., Watson, A.J., Weiss, R., Wong, C.S., Yoshikawa-Inoue, H., 2013. A uniform, quality controlled Surface Ocean CO2 Atlas (SOCAT). Earth Syst. Sci. Data 5, 125–143. https://doi.org/10.5194/essd-5-125-2013.

Pierrot, D., Lewis, E., Wallace, D.W.R., 2006. MS excel program developed for CO2 system calculations ORNL/CDIAC. Carbon Dioxide Inf. Anal. Cent., Oak Ridge Natl. Lab. U. S. Dept. of Energy, Oak Ridge, Tenn. https://cdiac.ess-dive.lbl.gov/ftp/co2sys/CO2SYS_calc_XLS_v2.1/. (Accessed 3 March 2022).

Poisson, A., Metzl, N., Brunet, C., Schauer, B., Bres, B., Ruiz-Pino, D., Louanchi, F., 1993. Variability of sources and sinks of CO2 in the western Indian and southern oceans during the year 1991. J. Geophys. Res. 98 (C12), 22759–22778. https://doi.org/10.1029/93JC02501.

Poulton, A.J., Stinchcombe, M.C., Quartly, G.D., 2009. High numbers of Trichodesmium and diazotrophic diatoms in the southwest Indian Ocean. Geophys. Res. Lett. 36, L15610. https://doi.org/10.1029/2009GL0397179.

Resplandy, L., Hogikyan, A., Müller, J.D., Najjar, R.G., Bange, H.W., Bianchi, D., et al., 2024. A synthesis of global coastal ocean greenhouse gas fluxes. Global Biogeochem. Cycles 38, e2023GB007803. https://doi.org/10.1029/2023GB007803.

Revelle, R., Suess, H.E., 1957. Carbon dioxide exchange between atmosphere and ocean and the question of an increase of atmospheric CO2 during the past decades. Tellus 9, 18–27. https://doi.org/10.1111/j.2153-3490.1957.tb01849.x.

Rödenbeck, C., Bakker, D.C.E., Gruber, N., Iida, Y., Jacobson, A.R., Jones, S., Landschützer, P., Metzl, N., Nakaoka, S., Olsen, A., Park, G.-H., Peylin, P., Rodgers, K.B., Sasse, T.P., Schuster, U., Shutler, J.D., Valsala, V., Wanninkhof, R., Zeng, J., 2015. Data-based estimates of the ocean carbon sink variability – First results of the Surface Ocean pCO2 Mapping intercomparison (SOCOM). Biogeosciences 12, 7251–7278. https://doi.org/10.5194/bg-12-7251-2015.

Roobaert, A., Regnier, P., Landschützer, P., Laruelle, G.G., 2024. A novel sea surface pCO2-product for the global coastal ocean resolving trends over 1982–2020. Earth Syst. Sci. Data 16, 421–441. https://doi.org/10.5194/essd-16-421-2024.

Sabine, C.L., Wanninkhof, R., Key, R.M., Goyet, C., Millero, F.J., 2000. Seasonal CO2 fluxes in the tropical and subtropical Indian Ocean. Mar. Chem. 72, 33–53. https://doi.org/10.1016/S0304-4203(00)00064-5.

Sarma, V.V.S.S., Krishna, M.S., Paul, Y.S., Murty, V.S.N., 2015. Observed changes in ocean acidity and carbon dioxide exchange in the coastal bay of Bengal—a link to air pollution. Tellus B 67 (1), 24638. https://doi.org/10.3402/tellusb.v67.24638.

Schlitzer, R., 2018. Ocean Data View.

Sridevi, B., Sarma, V., 2021. Role of river discharge and warming on ocean acidification and pco2 levels in the Bay of Bengal. Tellus B 73 (1), 1–20. https://doi.org/10.1080/16000889.2021.1971924.

Takahashi, T., Olafsson, J., Goddard, J.G., Chipman, D.W., Sutherland, S.C., 1993. Seasonal variation of CO2 and nutrients in the high-latitude surface oceans: a comparative study. Global Biogeochem. Cycles 7 (4), 843–878. https://doi.org/10.1029/93GB02263.

Takahashi, T., Sutherland, S.C., Wanninkhof, R., Sweeney, C., Feely, R.A., Chipman, D. W., Hales, B., Friederich, G., Chavez, F., Sabine, C., Watson, A.J., Bakker, D.C., Schuster, U., Metzl, N., Yoshikawa-Inoue, H., Ishii, M., Midorikawa, T., Nojiri, Y., Körtzinger, A., Steinhoff, T., Hoppema, M., Olafsson, J., Arnarson, T.S., Tilbrook, B., Johannessen, T., Olsen, A., Bellerby, R., Wong, C., Delille, B., Bates, N., de Baar, H.J., 2009. Climatological mean and decadal change in surface ocean pCO2, and net sea air CO2 flux over the global oceans. Deep-Sea Res. II 56 (8–10), 554–577. https://doi.org/10.1016/j.dsr2.2008.12.009.

Takahashi, T., Sutherland, S.C., Chipman, D.W., Goddard, J.G., Ho, C., Newberger, T., Sweeney, C., Munro, D.R., 2014. Climatological distributions of pH, pCO2, total CO2, alkalinity, and CaCO3 saturation in the global surface ocean, and temporal changes at selected locations. Mar. Chem. 164, 95–125. https://doi.org/10.1016/j.marchem.2014.06.004.

Touratier, F., Azouzi, L., Goyet, C., 2007. CFC-11, Δ14C and 3H tracers as a means to assess anthropogenic CO2 concentrations in the ocean. Tellus B 59 (2), 318–325. https://doi.org/10.1111/j.1600-0889.2006.00247.x.

Uppström, L.R., 1974. The boron/chlorinity ratio of deep-sea water from the Pacific Ocean. Deep Sea Research and Oceanographic Abstracts 21, 161–162. https://doi.org/10.1016/0011-7471(74)90074-6.

Wanninkhof, R., 1992. Relationship between wind speed and gas exchange over the ocean. J. Geophys. Res. 97 (C5), 7373–7382. https://doi.org/10.1029/92JC00188.

Wanninkhof, R., 2014. Relationship between wind speed and gas exchange over the ocean revisited. Limnol Oceanogr. Methods 12, 351–362. https://doi.org/10.4319/lom.2014.12.351.

Weiss, R.F., 1974. Carbon dioxide in water and seawater: the solubility of a non-ideal gas. Mar. Chem. 2, 203–215. https://doi.org/10.1016/0304-4203(74)90015-2.